manufacturer's instructions. The effect of siRNA on Gal-3 expression was observed using Western blotting with an anti–Gal-3/MAC-2 antibody (Cedarlane) and real-time PCR.

Migration Analysis

Migration analysis was performed using 5-μm pore-size cell culture inserts in 24-well plates (Corning, Chelmsford, UK). J774 cells or bone marrow–derived macrophages (1×10^4) were seeded into the top of the Transwell chambers precoated with fibronectin (Corning, Tokyo, Japan), and 8 μg/mL recombinant Gal-3 (R&D Systems, Minneapolis, MN) was added into the lower well. After 8 hours of incubation, cells on the upper membrane surface were removed with a cotton swab. Cells on the lower membrane surface were fixed with 4% formaldehyde and stained with Mounting Medium with DAPI (Vector Laboratories, Burlingame, CA).

In Vivo Tumor Cell Allograft Model

B16 or LLC tumor cells (1×10^6 per mouse in 0.1 mL PBS) were inoculated subcutaneously into wild-type C57BL/6 or *Gal3* KO mice (7 to 8 weeks of age). Tumors were dissected 18 days after implantation (in allografts using bone marrow–transplanted chimeric mice, discussed later (see *Bone Marrow Transplantation*)). Tumor volumes were measured with calipers every 3 days and were calculated as follows: width × width × length × 0.52.[18]

Immunohistochemistry

Immunostaining analysis was performed on 10-μm cryostat sections of mouse tumor tissue. Procedures for tissue fixation and staining of sections with antibodies were as described previously.[4] For immunohistochemistry, rat anti-mouse F4/80 antibody (AbD Serotec, Raleigh, NC), rat anti-mouse CD206 (MRC1) antibody (AbD Serotec), rat anti-mouse CD31 antibody (BD Pharmingen, San Jose, CA), and hamster anti-mouse CD31 antibody (Millipore) were used for staining and anti-rat IgG Alexa Fluor 488 (Invitrogen), anti-rat IgG Alexa Fluor 546 (Invitrogen), and anti-Armenian hamster FITC (eBioscience, San Diego, CA) as the secondary antibodies. Cell nuclei were visualized with TO-PRO-3 (Invitrogen). To measure hypoxia in tumor tissues, 60 mg/kg HypoxyProbe-1 (Hypoxyprobe, Inc, Burlington, MA) was injected intraperitoneally 1 hour before sacrificing the mice. Tumor sections were stained using an anti-HypoxyProbe antibody. Sections were observed by conventional microscopy (brightfield) (DM5500 B; Leica, Wetzlar, Germany) or confocal microscopy (TCS/SP5; Leica), and images were acquired with a digital camera (DFC500; Leica). In all analyses, an isotype-matched control Ig was used as a negative control and it was confirmed that the positive signals were not derived from a nonspecific background. Images were processed using Photoshop CS2 software version 9.0.2 (Adobe Systems, San Jose, CA). All images shown are representative of six or more independent experiments.

Flow Cytometry

Flow cytometric analysis was performed as described previously.[5] Fluorescence-labeled anti-mouse antibodies specific for F4/80, CD206 (MRC1) (AbD Serotec), CD11b, and CD45 (BD Pharmingen) were used. Stained cells were analyzed with a FACSCalibur or FACSAria (BD Biosciences) using FlowJo software version 7.6.1 (TreeStar, Ashland, OR) and sorted by a FACSAria. Dead cells were excluded by propidium iodide staining or analyses using the two-dimensional profile of the forward versus side scatter.

Bone Marrow Transplantation

Bone marrow cells from wild-type mice were transplanted into wild-type C57BL/6 or *Gal3* KO mice (7 to 8 weeks of age). Bone marrow cells were obtained by flushing the tibias and femurs of age-matched donor wild-type C57BL/6 mice. Bone marrow transplantation (BM-T) was performed using lethally irradiated (10.0 Gy) wild-type C57BL/6 or *Gal3* KO mice by intravenous infusion of 1×10^6 donor whole bone marrow cells. Four weeks after transplantation, BM chimeric mice received an inoculation of B16 or LLC tumor cells (1×10^6 per mouse in 0.1 mL PBS) subcutaneously, and tumor tissues were dissected 18 days after implantation. Tumor volumes were measured with calipers every 3 days and calculated as follows: width × width × length × 0.52.[18]

Statistical Analysis

All data are presented as means ± SD. Statistical analysis was performed by the Tukey-Kramer multiple comparison test using the statcel version 2 software package (OMS, Saitama, Japan). When only two groups were compared, a two-sided Student's *t*-test was used. A P value less than 0.05 was considered statistically significant.

Results

Tumor Growth Is Enhanced in *Gal3*$^{-/-}$ Mice

It has been suggested that Gal-3 induces angiogenesis by directly promoting chemotaxis of ECs.[19] Functional chemotaxis also may involve other cell types, such as monocytes/macrophages, because of the known function of Gal-3 in macrophage migration.[13,20] Macrophages act as proangiogenic accessory cell components in tumors by secreting several angiogenic factors such as vascular endothelial growth factor, matrix metalloproteinases, and others.[21–23] Therefore, it was hypothesized that Gal-3 in the tumor environment accelerates tumor angiogenesis via macrophage chemotaxis, resulting in tumor growth. To test this, *Gal3* mutant (*Gal3*$^{-/-}$) mice were used as tumor-bearing hosts because macrophages themselves

produce Gal-3 and chemotaxis caused by tumor-derived Gal-3 would not be assessable. Although Gal-3 production from tumor stromal cells is absent in *Gal3*$^{-/-}$ mice, tumor cell–derived Gal-3 should generate a concentration gradient from the tumor, enabling visualization of *Gal3*-deficient macrophage infiltration into tumor tissue.

We used two cancer cell lines, B16 mouse melanoma and LLC mouse lung cancer cells for the allograft model. We inoculated these cells into *Gal3*$^{+/+}$ (wild-type) and *Gal3*$^{-/-}$ mice and evaluated tumor growth. These results showed enhancement of tumor growth in *Gal3*$^{-/-}$ mice compared with *Gal3*$^{+/+}$ mice in both B16 (Figure 1, A–C) and LLC tumors (Figure 1, D–F).

Macrophage Migration Is Induced by Gal-3

Both B16 and LLC tumor tissues were found to express Gal-3 more strongly than normal cells such as those from skin, spleen (B cells), liver, and lung, both at the mRNA (Figure 1G) and protein levels (Figure 1H). This suggests that cancer cell–derived Gal-3 does form a concentration gradient in *Gal3*$^{-/-}$ mice and may induce migration of monocytes/macrophages into tumors. The number of infiltrated F4/80-positive macrophage lineage cells was significantly higher in tumors that developed in *Gal3*$^{-/-}$ mice than in *Gal3*$^{+/+}$ mice (Figure 2, A and B).

Next, we investigated if exogenous Gal-3 induces chemotaxis of macrophages and if endogenous Gal-3 in macrophages would obscure this chemotaxis. We used J774, a macrophage cell line, and silenced Gal-3 expression by siRNA (Figure 2C). As expected, knockdown of endogenous Gal-3 enhanced transmigration of J774 macrophages (Figure 2, D and E).

We next isolated CD45^{high} CD11b^{high} F4/80^{high} macrophages from the bone marrow of *Gal3*$^{+/+}$ or *Gal3*$^{-/-}$ mice and confirmed a lack of Gal-3 in those from *Gal3* KO animals (Figure 2F). By using these primary macrophages, we observed chemotaxis stimulated by Gal-3. As was seen in the J774 cell line, a lack of endogenous Gal-3 resulted in enhanced macrophage chemotaxis along a Gal-3 gradient (Figure 2, G and H).

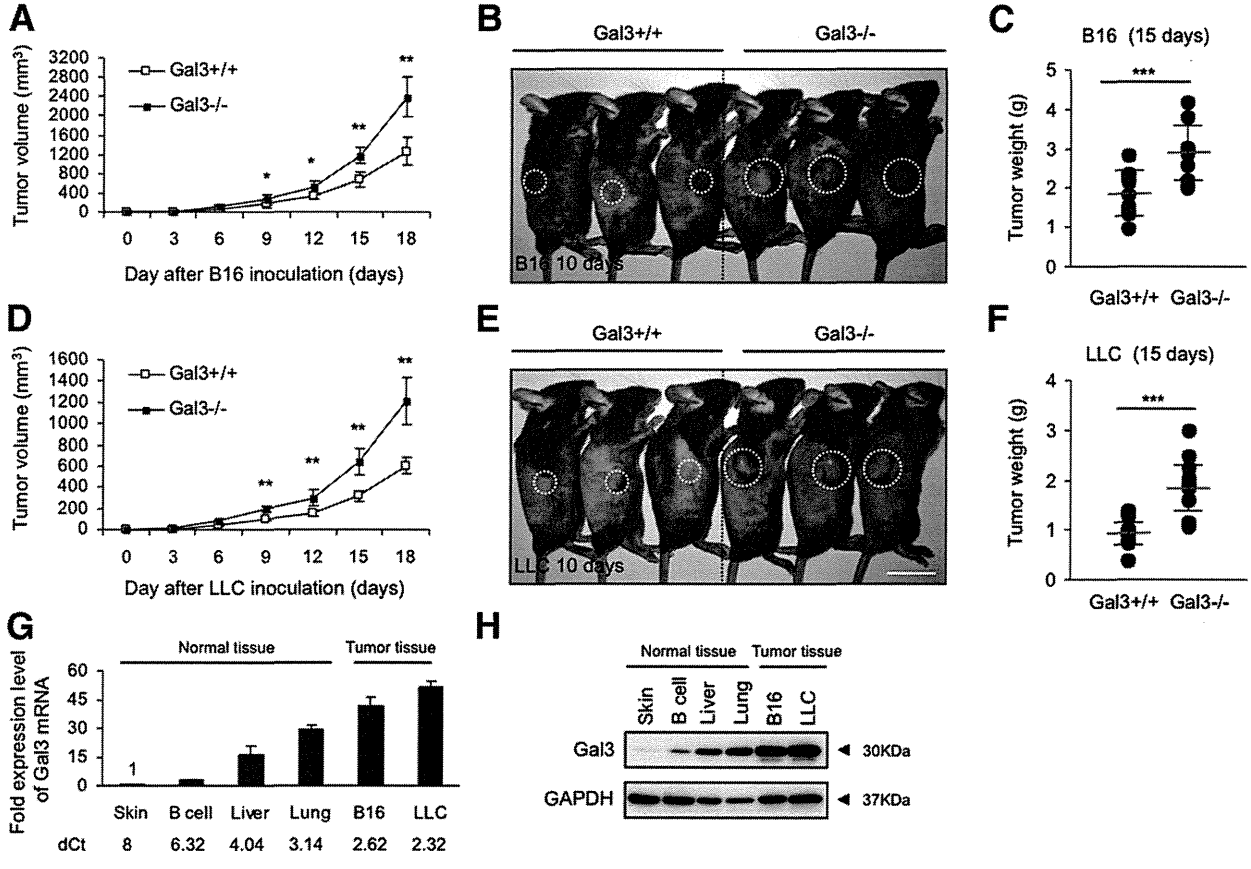

Figure 1 Tumor growth *Gal3*$^{-/-}$ mice. **A:** Tumor growth curves of B16 (melanoma) cells on s.c. injection into *Gal3*$^{+/+}$ (wild-type) or *Gal3*$^{-/-}$ (KO) mice ($n = 10$ for each group). Data are means ± SEM. $^{*}P < 0.05$, $^{**}P < 0.01$. **B:** Gross appearance of tumors derived from B16 cells on day 10 after tumor cell inoculation. **Dashed lines** indicate tumor area. Scale bar = 2 cm. **C:** Tumor weight on day 15 after B16 cell inoculation ($n = 10$). Data are means ± SEM. $^{***}P < 0.001$. **D:** Tumor growth curves of LLC cells on s.c. injection into *Gal3*$^{+/+}$ or *Gal3*$^{-/-}$ mice ($n = 10$ for each group). Data are means ± SEM. $^{**}P < 0.01$. **E:** Gross appearance of tumors derived from LLC cells on day 10 after tumor cell inoculation. **Dashed lines** indicate tumor area. Scale bar = 2 cm. **F:** Tumor weight on day 15 after LLC cell inoculation ($n = 10$). Data are means ± SEM. $^{***}P < 0.001$. **G:** Quantitative real-time PCR analysis of Gal-3 mRNA expression in tumor (B16, LLC) and normal tissue-derived single-cell suspensions (total skin, liver, lung, or B cell from spleen). Threshold values for target genes normalized against the level of glyceraldehyde-3-phosphate dehydrogenase (GAPDH) **ΔCT** values (dCT) are shown under the graph ($n = 3$). **H:** Western blot analysis of Gal-3 expression in whole-cell extracts of tumor (B16, LLC) and normal tissue-derived single-cell suspensions (total skin, liver, lung, or B cell from spleen) with anti–Gal-3/Mac2 and anti-GAPDH antibodies.

M2 Macrophage Infiltration Is Enhanced in Tumors Developing in *Gal3*$^{-/-}$ Mice

Because we found abundant F4/80-positive macrophage lineage cells migrating into tumors developing in *Gal3*$^{-/-}$ mice, we identified their subtype. We confirmed that a population of CD11b^{high} F4/80^{high} macrophages was more highly abundant in both B16 and LLC tumors developing in *Gal3*$^{-/-}$ mice than in *Gal3*$^{+/+}$ mice (Figure 3A). Macrophages in tumors from *Gal3*$^{-/-}$ mice expressed MRC1 (CD206), an M2 macrophage marker, more strongly than in *Gal3*$^{+/+}$ mice (Figure 3B). Moreover, they expressed IL10 and monocyte chemoattractant protein-1 strongly as well as MRC1 at the mRNA level, a characteristic M2 macrophage gene signature (Figure 3C).[24] LLC but not B16 tumors in *Gal3*$^{+/+}$ mice expressed tumor necrosis factor-α more abundantly than in *Gal3*$^{-/-}$ mice. M2 macrophages were more abundant in LLC than B16 tumors. Therefore, M1 macrophage-mediated effects may be more apparent in LLC tumors of *Gal3*$^{+/+}$ mice.

The earlier-described data suggest that cells similar to M2 macrophages may migrate selectively into the tumor parenchyma when Gal-3 production is higher in the tumor than in nontumor tissue, such that a concentration gradient occurs. Moreover, it was possible that Gal-3 expression in M2 macrophages was constitutively lower and they more easily migrated into Gal-3-producing areas. We therefore divided bone marrow CD11b^{high} F4/80^{high} macrophages into two fractions, that is, MRC1^{low} and MRC1^{high} (Figure 3D), and quantified their Gal-3 expression (Figure 3E). MRC1 mRNA expression correlated with the protein level in macrophages. As expected, Gal-3 mRNA expression was lower in MRC1^{high} than in MRC1^{low} macrophages.

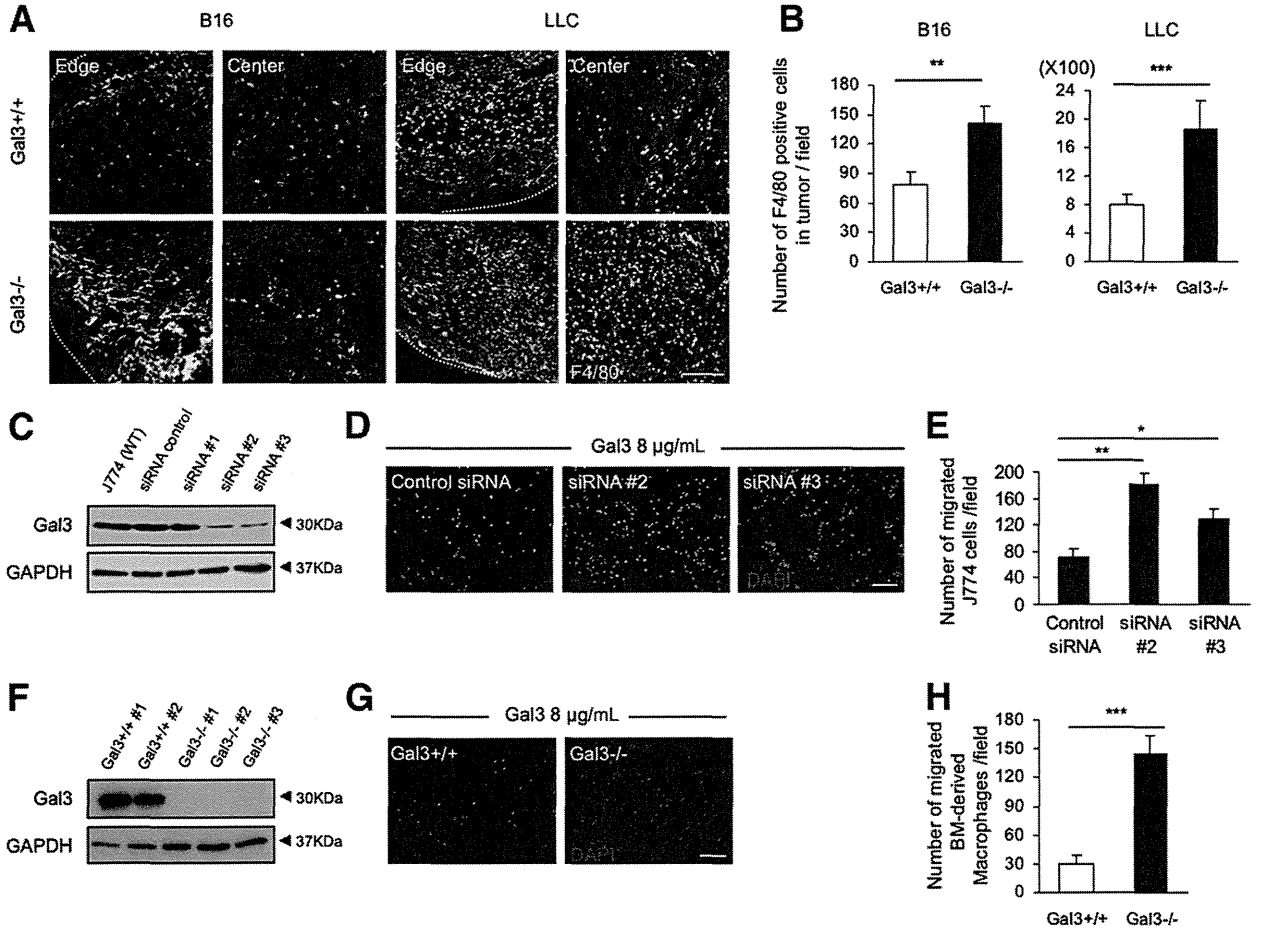

Figure 2 Migration of macrophages stimulated by Gal-3. **A:** Immunofluorescence staining of F4/80 (green) and TO-PRO-3 (blue) in the B16 or LLC tumor sections from *Gal3*$^{+/+}$ or *Gal3*$^{-/-}$ mice. Scale bar = 200 μm. **B:** Quantitative evaluation of migrated F4/80-positive macrophages in B16 or LLC tumors. Data are means ± SEM. $^{**}P < 0.01$, $^{***}P < 0.001$ (five random fields of 10 independent tumor sections). **C:** Western blot analysis of Gal-3 expression in J774 cells after silencing by RNA interference. Three different Gal-3-specific siRNAs (siRNA#1, siRNA#2, and siRNA#3) and control siRNA were used. **D:** Migration analysis using the Transwell technique. Representative images of migrated J774 cells stained with DAPI. Scale bar = 200 μm. **E:** Quantification of migrated J774 cells from five random fields of four independent samples. Data are means ± SEM. $^{*}P < 0.05$, $^{**}P < 0.01$. **F:** Western blot analysis of Gal-3 expression in bone marrow–derived macrophages (CD45^{high} CD11b^{high} F4/80^{high}) from *Gal3*$^{+/+}$ or *Gal3*$^{-/-}$ mice. Numbers 1, 2, and 3 are different individual mice. **G:** Migration analysis using bone marrow–derived macrophages as in **F**. Representative images of migrated cells stained with DAPI are shown. Scale bar = 200 μm. **H:** Quantification of migrated bone marrow–derived macrophages from five random fields of four independent samples. Data are means ± SEM. $^{***}P < 0.001$. GAPDH, glyceraldehyde-3-phosphate dehydrogenase.

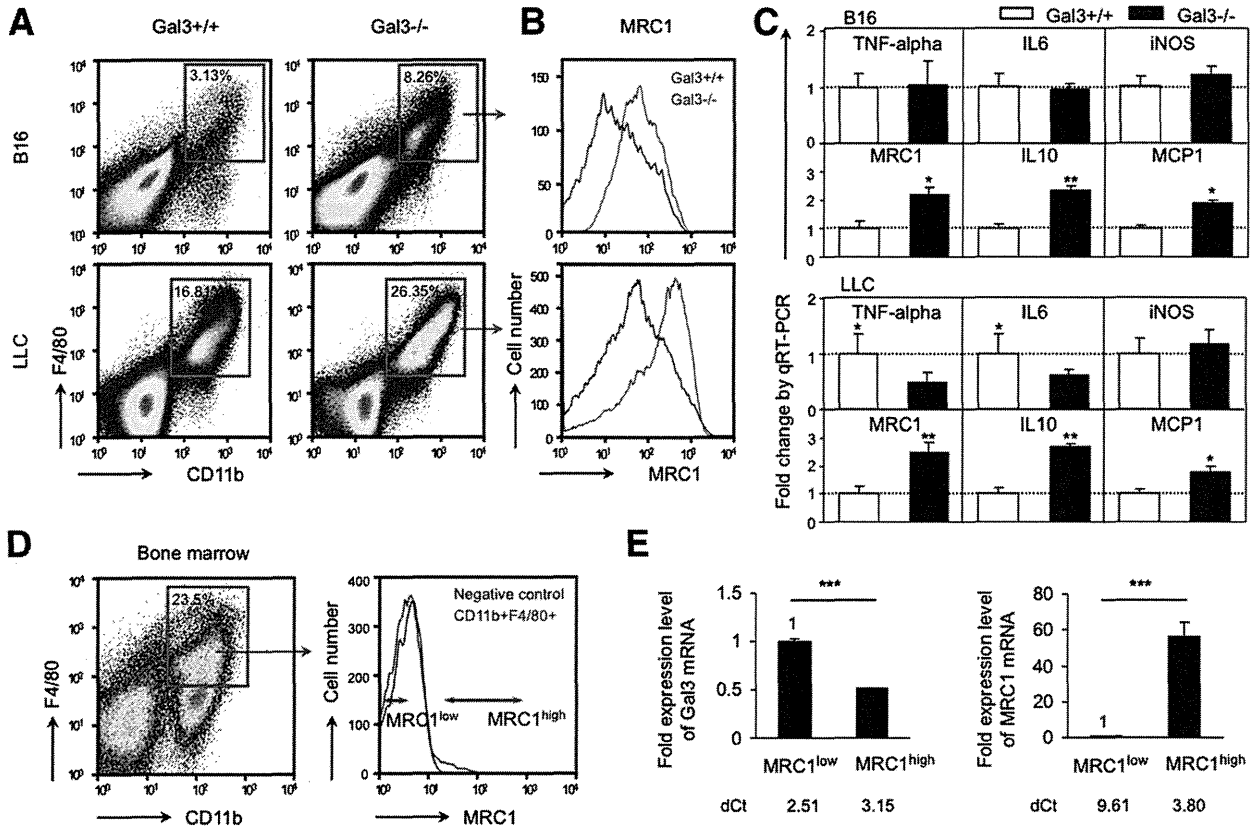

Figure 3 Increased M2 macrophage migration in *Gal3*$^{-/-}$ mice. **A:** Flow cytometric analysis of CD11b^{high} F4/80^{high} macrophages in B16 or LLC tumors in *Gal3*$^{+/+}$ or *Gal3*$^{-/-}$ mice. The population of CD11b^{high} F4/80^{high} macrophages within total cells in the tumor is shown in the gated **red box. B:** Histogram showing MRC1 expression intensity in the CD11b^{high} F4/80^{high} macrophages gated by the **red box** in **A.** Flow cytometric analysis was performed on day 12 after tumor cell implantation. Data are representative of B16 (n = 18) or LLC (n = 24) tumors. **C:** Quantitative real-time PCR analysis of mRNA expression in CD45^{high} CD11b^{high} F4/80^{high}-expressing tumor macrophages in B16 or LLC tumors in *Gal3*$^{+/+}$ or *Gal3*$^{-/-}$ mice. Data are means ± SEM. $*P < 0.05$, $**P < 0.01$ (n = 5). **D** and **E:** Analysis of Gal-3 expression in bone marrow–derived MRC1^{low} and MRC1^{high} macrophages from WT mice. **D:** Representative flow cytometric plots of cells from bone marrow of WT mice. **Left:** CD11b^{high} F4/80^{high} macrophage fraction is gated by the **red box** (23.5% ± 2.58%). **Right:** Histogram showing MRC1 expression intensity in CD11b^{high} F4/80^{high} macrophages. MRC1^{low} and MRC1^{high} macrophages were sorted as indicated (**right**). **E:** Quantitative real-time PCR analysis of Gal-3 and MRC1 mRNA expression in MRC1^{low} and MRC1^{high} macrophages sorted as in **C.** Threshold values for target genes normalized against the level of glyceraldehyde-3-phosphate dehydrogenase (**ΔCT** values; dCt) are shown under the graph. Data are means ± SEM. $***P < 0.001$ (n = 4). iNOS, inducible nitric oxide synthase; MCP1, monocyte chemoattractant protein-1; TNF, tumor necrosis factor.

Tumor Angiogenesis Is Enhanced in Tumors Developing in *Gal3*$^{-/-}$ Mice

It is widely accepted that M2 macrophages promote angiogenesis.[25,26] Therefore, enhanced tumor growth in *Gal3*$^{-/-}$ is suggested to be induced by increased angiogenesis as a result of infiltration by M2-like macrophages. Hence, we investigated the localization of MRC1-positive macrophages in the tumor microenvironment. As shown in Figure 4, A–C, higher numbers of MRC-positive macrophages were observed in both B16 and LLC tumors developing in *Gal3*$^{-/-}$ than in *Gal3*$^{+/+}$ mice. Moreover, co-localization of MRC1-positive cells with CD31-positive ECs indicated that more of these cells were interacting with blood vessels in both B16 and LLC tumors in *Gal3*$^{-/-}$ mice.

The number of blood vessels identified as CD31^{+} was significantly higher in both B16 and LLC tumors developing in *Gal3*$^{-/-}$ than in *Gal3*$^{+/+}$ mice (Figure 4, D and E). It is possible that a mere increase in the number of blood vessels does not necessarily correlate with effective blood circulation in tumors and that nonfunctional blood vessel formation increases severe hypoxia.[27] We therefore evaluated hypoxic conditions and found that hypoxia was not more severe in tumors developing in *Gal3*$^{-/-}$ mice (Figure 4, F and G), suggesting that functional blood vessels are induced in tumors in *Gal3*$^{-/-}$ mice, enhancing tumor growth.

Restoration of Gal-3 in Bone Marrow Cells of *Gal3*$^{-/-}$ Mice Abrogates Enhanced Tumor Growth

Lack of Gal-3 in bone marrow macrophage lineage cells may be responsible for the enhancement of M2-like macrophage infiltration into tumors, resulting in induction of tumor angiogenesis and enhanced tumor growth. To test this hypothesis, we replaced the bone marrow of *Gal3*$^{-/-}$ mice with cells from *Gal3*$^{+/+}$ mice by BM-T and analyzed tumor growth and angiogenesis using these chimeric mice [*Gal3*$^{-/-}$ (BM-T)

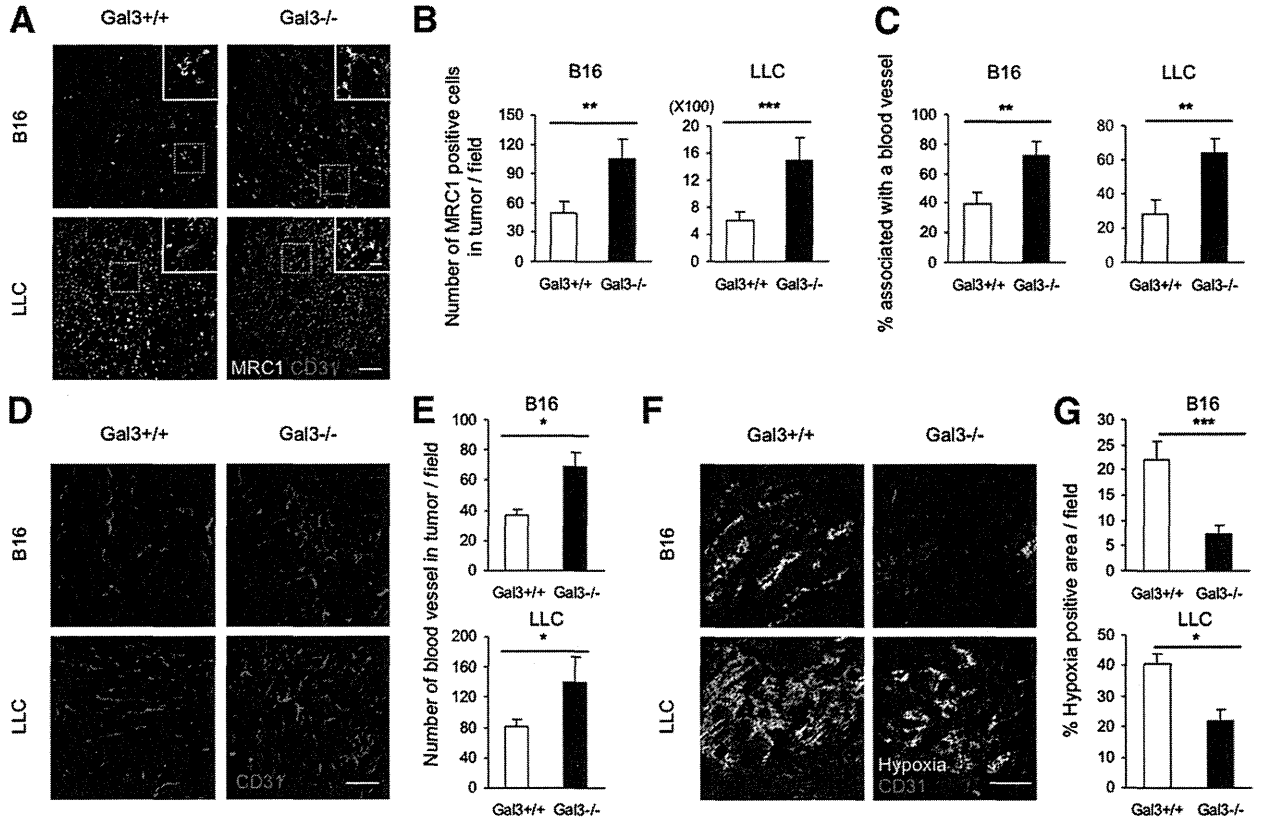

Figure 4 Increased tumor angiogenesis with M2 macrophage infiltration in $Gal3^{-/-}$ mice. **A:** Immunofluorescence staining of MRC1 (green) and CD31 (red) in the B16 or LLC tumor sections from $Gal3^{+/+}$ or $Gal3^{-/-}$ mice. **Dashed boxes** indicate areas shown at higher magnification. **Arrows** indicate focal MRC1-positive cells closely localizing to blood vessels. Scale bar = 100 μm and 25 μm (**inset**). **B:** Quantitative evaluation of the number of MRC1-positive macrophages in B16 tumor (**left**) or LLC tumor (**right**) sections from $Gal3^{+/+}$ or $Gal3^{-/-}$ mice. Data are means ± SEM. $^{**}P < 0.01$, $^{***}P < 0.001$ (five random fields of four independent tumor sections). **C:** Percentage of MRC1-positive macrophages closely localizing to blood vessels in B16 tumor (**left**) or LLC tumor (**right**) sections from $Gal3^{+/+}$ or $Gal3^{-/-}$ mice. Data are means ± SEM. $^{**}P < 0.01$ (five random fields of four independent tumor sections). **D:** Immunofluorescence staining of CD31 (red) in the B16 or LLC tumor sections derived from $Gal3^{+/+}$ or $Gal3^{-/-}$ mice. Scale bar = 200 μm. **E:** Quantification of the number of blood vessels as in **D**. Data are means ± SEM. $^{*}P < 0.05$ (five random fields of four independent tumor sections). **F:** Immunofluorescence staining of CD31 (red) in the B16 or LLC tumor sections from $Gal3^{+/+}$ or $Gal3^{-/-}$ mice. Hypoxic status was revealed by HypoxyProbe (green). Scale bar = 500 μm. **G:** Quantification of the hypoxic area in B16 or LLC tumor sections from $Gal3^{+/+}$ or $Gal3^{-/-}$ mice. Data are means ± SEM. $^{*}P < 0.05$, $^{***}P < 0.001$ (five random fields of 10 independent tumor sections).

mice] (Figure 5A). We generated control mice in which bone marrow of $Gal3^{+/+}$ animals was replaced with that of $Gal3^{+/+}$ mice [$Gal3^{+/+}$ (BM-T) mice].

After BM-T, we confirmed that bone marrow cells did express Gal-3 in the $Gal3^{-/-}$ (BM-T) mice (Figure 5B). Enhancement of both B16 and LLC tumor growth was abrogated completely in $Gal3^{-/-}$ (BM-T) mice (Figure 5, C–H). In terms of macrophage infiltration, the number of F4/80-positive cells in the tumor microenvironment was not significantly different between $Gal3^{-/-}$ (BM-T) mice and $Gal3^{+/+}$ (BM-T) mice (Figure 6, A and B). This was also the case when the number of MRC1-positive cells and the number of these cells closely associating with CD31-positive blood vessels in the tumor microenvironment was quantified (Figure 6, C–E). Attenuation of enhancement of macrophage infiltration into tumors developing in $Gal3^{-/-}$ (BM-T) mice also was accompanied by restoration of angiogenesis to a level observed in $Gal3^{+/+}$ (BM-T) host tumors (Figure 6, C–E). Therefore, we conclude that lack of Gal-3 in bone marrow cells is responsible for the enhanced migration of macrophages into the tumor microenvironment, and that this facilitates tumor growth.

Discussion

We analyzed the functional role of tumor environmental Gal-3 in tumor growth. Although several functions of Gal-3 in a variety of cells, such as immune cells, neuronal cells, epithelial cells, cancer cells, and others, have been suggested,[12,28] we focused on macrophages. It has been reported that recombinant Gal-3 induces chemotaxis of monocytes/macrophages; however, the *in vivo* relevance of this for tumor growth had not been analyzed. We report that Gal-3 produced by the tumor induces macrophage migration, resulting in the promotion of angiogenesis and tumor growth.

There are two modes of action of Gal-3 (ie, mediated by intracellular Gal-3), especially in the nucleus, or secreted

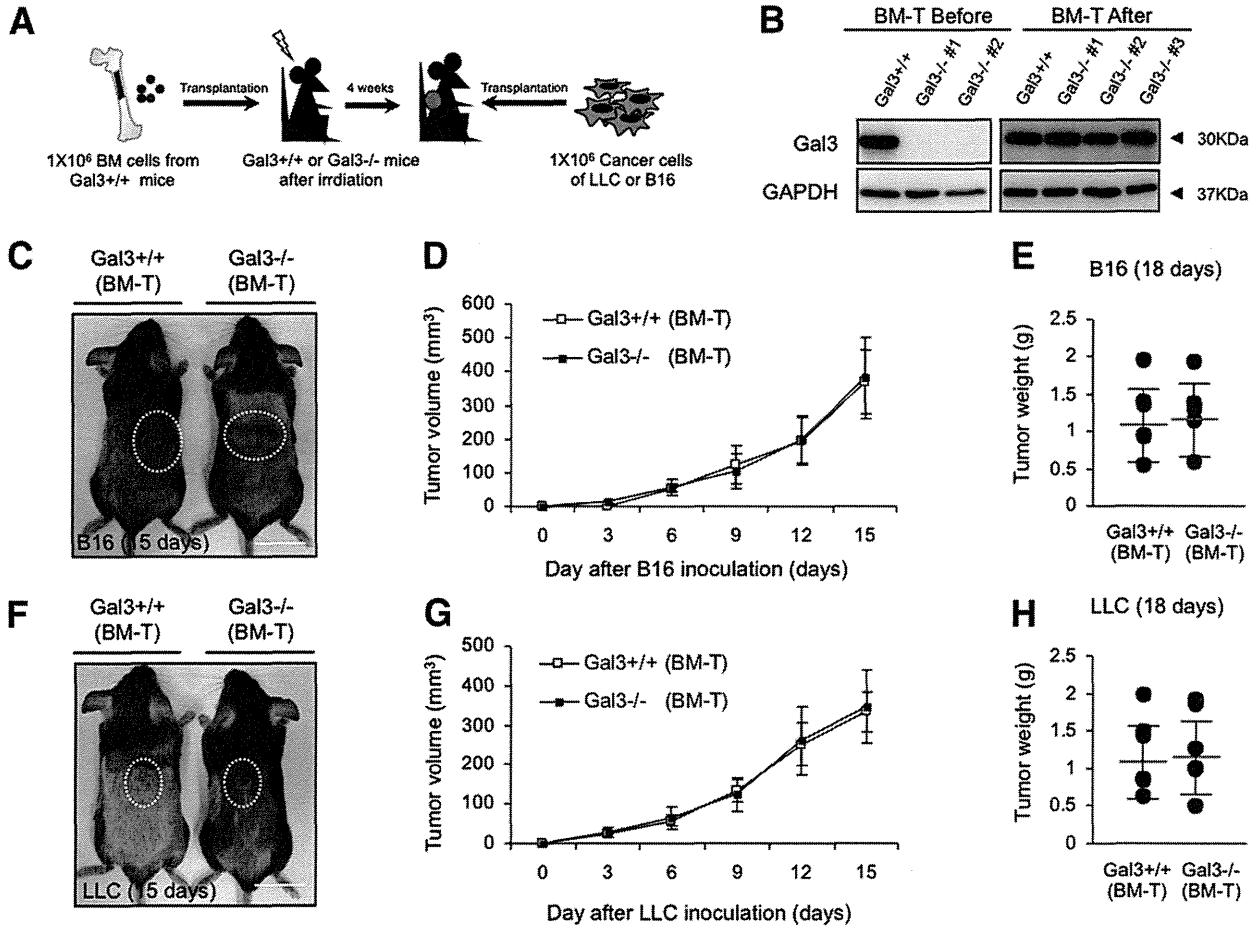

Figure 5 Tumor growth in *Gal3*$^{-/-}$ mice transplanted with wild-type bone marrow cells. **A:** The experimental scheme of BM-T and the tumor cell allograft model. For details, see *Materials and Methods*. **B:** Western blot analysis of Gal-3 expression in bone marrow cells 4 weeks after BM-T in *Gal3*$^{-/-}$ mice as in **A**. Numbers 1, 2, and 3 are different individual mice. Bone marrow cells from *Gal3*$^{+/+}$ mice were used as the positive control. **C:** Gross appearance of B16 tumors developing in BM-T–treated *Gal3*$^{+/+}$ and *Gal3*$^{-/-}$ mice on day 15 after tumor cell inoculation. **Dashed lines** indicate tumor area. Scale bars: 2 cm. **D:** Tumor growth curves of B16 cells on s.c. injection into *Gal3*$^{+/+}$ (BM-T) or *Gal3*$^{-/-}$ (BM-T) mice as in **C** (n = 10). **E:** Tumor weight 18 days after B16 cell inoculation as in **C** (n = 7). **F:** Gross appearance of LLC tumors developing in BM-T–treated *Gal3*$^{+/+}$ and *Gal3*$^{-/-}$ mice on day 15 after tumor cell inoculation. **Dashed lines** indicate tumor area. Scale bars: 2 cm. **G:** Tumor growth curves of LLC cells on s.c. injection into *Gal3*$^{+/+}$ (BM-T) or *Gal3*$^{-/-}$ (BM-T) mice as in **F** (n = 10). **H:** Tumor weight 18 days after LLC cell inoculation as in **F** (n = 7). Data are means ± SEM. GAPDH, glyceraldehyde-3-phosphate dehydrogenase.

Gal-3. In the case of intracellular action, Gal-3 as a component of the heterogeneous nuclear ribonuclear protein is a factor in pre-mRNA splicing to control cell cycling and prevent apoptosis possibly mediated through interaction with Bcl-2 family members.[29,30] On the other hand, the secreted form of Gal-3 regulates cell adhesion and migration through cell-cell and cell-extracellular matrix interactions.[31,32] In terms of myeloid cell lineages, it has been reported that exogenous Gal-3 affects apoptosis of neutrophils in a context-dependent manner[33] and induces mediator release from both IgE-sensitized and IgE-nonsensitized mast cells.[34,35] Here, we analyzed Gal-3 secreted from tumors for its action on macrophages. It has been reported that Gal-3 production is observed in immune cells, epithelial cells, and neuronal cells.[12,31] To analyze the migration of macrophages into the tumor microenvironment more precisely, attenuation of Gal-3 expression by all cells except tumor cells is required. In our system, we used *Gal3*$^{-/-}$ mice as an allograft host and two Gal-3-producing cancer cell lines that established tumors generating a concentration gradient of Gal-3, enabling us to visualize macrophage migration.

Macrophages in the tumor microenvironment are termed tumor-associated macrophages and their number correlates with the malignancy of the tumor.[36] It is widely accepted that tumor-associated macrophages promote angiogenesis, which stimulates tumor growth.[25,26] In our present work, we found that the Gal-3 concentration gradient effectively induced migration of M2-like macrophages. It is well known that there are two types of macrophages. One is termed M1, which are macrophages differentiated and activated by lipopolysaccharide and the proinflammatory cytokine interferon-γ. M1 macrophages produce high levels of oxidative metabolites and proinflammatory cytokines for host defense and tumor cell death.[37,38] On the other hand, M2 macrophages activated by IL4 or IL13 promote angiogenesis and also matrix remodeling.[39–41] Therefore, a high frequency of M2 macrophages as observed in tumors developing in *Gal3*$^{-/-}$ mice correlates with robust angiogenesis in this model.

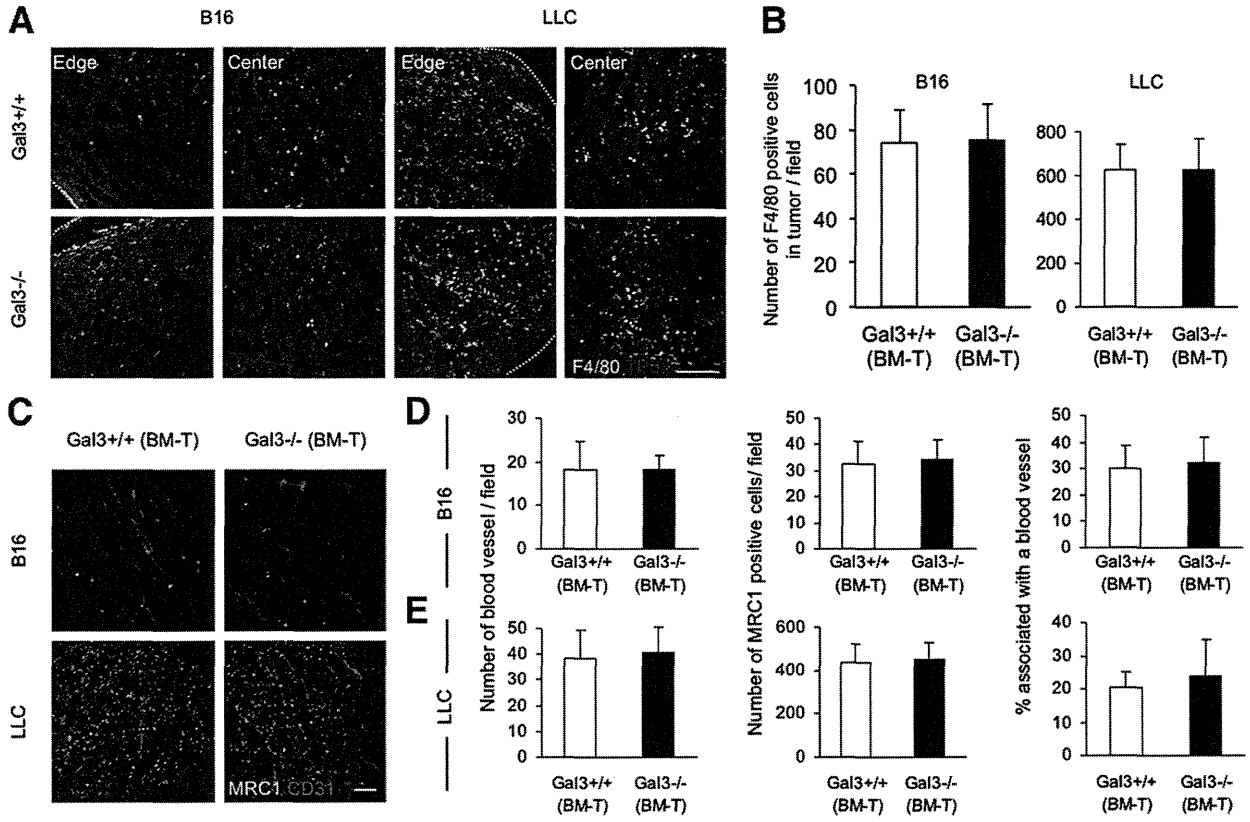

Figure 6 Infiltration of macrophages and tumor angiogenesis in *Gal3*$^{-/-}$ mice transplanted with WT bone marrow cells. **A**: Immunofluorescence staining of F4/80 (green) and TO-PRO-3 (blue) in the B16 or LLC tumor sections from *Gal3*$^{+/+}$ (BM-T) or *Gal3*$^{-/-}$ (BM-T) mice as in Figure 5C. Scale bars: 200 μm. **B**: Quantification of the number of F4/80-positive macrophages in B16 or LLC tumor sections from *Gal3*$^{+/+}$ (BM-T) or *Gal3*$^{-/-}$ (BM-T) mice. Data are means ± SEM (five random fields of seven independent tumor sections). **C**: Immunofluorescence staining of MRC1 (green) and CD31 (red) in the B16 or LLC tumor sections from *Gal3*$^{+/+}$ (BM-T) or *Gal3*$^{-/-}$ (BM-T) mice. Scale bars: 100 μm. **D** and **E**: Quantification of the number of blood vessels (**left**), of MRC1-positive macrophages (**middle**), and of MRC1-positive cells closely associating with blood vessels (**right**) in B16 (**D**) or LLC (**E**) tumor sections from *Gal3*$^{+/+}$ (BM-T) or *Gal3*$^{-/-}$ (BM-T) mice. Data are means ± SEM (five random fields of seven independent tumor sections).

Interestingly, we found that MRC1-positive M2-like macrophages express lower levels of Gal-3 than MRC-negative macrophages. When cells abundantly express Gal-3, they may not use remotely produced Gal-3 for their chemoattractive migration toward the Gal-3-producing area. Therefore, Gal-3 expression needs to be attenuated for testing cell migration toward Gal-3. In our analysis, J774 macrophages in which Gal-3 had been knocked down, or macrophages from *Gal3*$^{-/-}$ mice, more effectively migrate toward Gal-3 than the parental J774 cells or macrophages derived from *Gal3*$^{+/+}$ mice, respectively. These results suggest that M2 macrophages have the ability to migrate along Gal-3 concentration gradients.

In our present model, we injected LLC lung cancer cells subcutaneously, so this was a nonorthotopic model. Because melanoma occurs in the skin, subcutaneous B16 injection may be viewed as an orthotopic model. In tumor progression, interactions between host cells and tumor cells influence both angiogenesis and metastasis.[42] Therefore, in addition to the nonorthotopic model using LLC cells, we inoculated these cells into the lung and observed the effects of Gal-3. The results suggest that Gal-3 from tumor cells induces migration of M2 macrophages and angiogenesis in an orthotopic model (Supplemental Figure S1[43]). This further suggests that Gal-3 from metastatic as well as primary tumor induces macrophage migration into the tumor.

Our present model using *Gal3*$^{-/-}$ mice as a tumor host recapitulates the tumor condition in which expression of Gal-3 in the tumor increases. It has been reported that Gal-3 directly induces endothelial tube formation.[19,44] Therefore, higher levels of Gal-3 induce angiogenesis directly affecting ECs within the tumor; however, macrophage recruitment by Gal-3 also may be involved in the acceleration of tumor angiogenesis. In summary, knowledge of Gal-3 expression may help in the assessment of cancer patient status. Indeed, one line of evidence suggests that Gal-3 expression levels are related to the degree of biological aggressiveness in human colorectal tumors.[45] Therefore, suppression of the function or expression of Gal-3 may be a promising approach for cancer therapy.

Acknowledgments

We thank Dr. Daniel K. Hsu, Dr. Fu-Tong Liu (University of California), and Dr. Koichi Hiraga (University of

Toyama, Japan) for providing *Gal3*$^{-/-}$ mice; Noriko Fujimoto for preparation of plasmid DNA; and Keisho Fukuhara for administrative assistance.

Supplemental Data

Supplemental material for this article can be found at *http://dx.doi.org/10.1016/j.ajpath.2013.01.017.*

References

1. Carmeliet P: Angiogenesis in health and disease. Nat Med 2003, 9: 653–660
2. Carmeliet P: Angiogenesis in life, disease and medicine. Nature 2005, 438:932–936
3. Coussens LM, Werb Z: Inflammation and cancer. Nature 2002, 420: 860–867
4. Takakura N, Watanabe T, Suenobu S, Yamada Y, Noda T, Ito Y, Satake M, Suda T: A role for hematopoietic stem cells in promoting angiogenesis. Cell 2000, 102:199–209
5. Yamada Y, Takakura N: Physiological pathway of differentiation of hematopoietic stem cell population into mural cells. J Exp Med 2006, 203:1055–1065
6. Kessenbrock K, Plaks V, Werb Z: Matrix metalloproteinases: regulators of the tumor microenvironment. Cell 2010, 141:52–67
7. Coffelt SB, Tal AO, Scholz A, De Palma M, Patel S, Urbich C, Biswas SK, Murdoch C, Plate KH, Reiss Y, Lewis CE: Angiopoietin-2 regulates gene expression in TIE2-expressing monocytes and augments their inherent proangiogenic functions. Cancer Res 2010, 70: 5270–5280
8. Mazzieri R, Pucci F, Moi D, Zonari E, Ranghetti A, Berti A, Politi LS, Gentner B, Brown JL, Naldini L, De Palma M: Targeting the ANG2/TIE2 axis inhibits tumor growth and metastasis by impairing angiogenesis and disabling rebounds of proangiogenic myeloid cells. Cancer Cell 2011, 19:512–526
9. Qian BZ, Pollard JW: Macrophage diversity enhances tumor progression and metastasis. Cell 2010, 141:39–51
10. Grivennikov SI, Greten FR, Karin M: Immunity, inflammation, and cancer. Cell 2010, 140:883–899
11. Barondes SH, Castronovo V, Cooper DN, Cummings RD, Drickamer K, Feizi T, Gitt MA, Hirabayashi J, Hughes C, Kasai K, Leffler H, Liu F, Lotan R, Mercurio AM, Monsigny M, Pillai S, Poirer F, Raz A, Rigby PW, Rini JM, Wang JL: Galectins: a family of animal beta-galactoside-binding lectins. Cell 1994, 76:597–598
12. Dumic J, Dabelic S, Flögel M: Galectin-3: an open-ended story. Biochim Biophys Acta 2006, 1760:616–635
13. Sano H, Hsu DK, Yu L, Apgar JR, Kuwabara I, Yamanaka T, Hirashima M, Liu FT: Human galectin-3 is a novel chemoattractant for monocytes and macrophages. J Immunol 2000, 165:2156–2164
14. Radosavljevic G, Volarevic V, Jovanovic I, Milovanovic M, Pejnovic N, Arsenijevic N, Hsu DK, Lukic ML: The roles of Galectin-3 in autoimmunity and tumor progression. Immunol Res 2012, 52: 100–110
15. Hsu DK, Yang RY, Pan Z, Yu L, Salomon DR, Fung-Leung WP, Liu FT: Targeted disruption of the galectin-3 gene results in attenuated peritoneal inflammatory responses. Am J Pathol 2000, 156: 1073–1083
16. Naito H, Kidoya H, Sakimoto S, Wakabayashi T, Takakura N: Identification and characterization of a resident vascular stem/progenitor cell population in preexisting blood vessels. EMBO J 2011, 31: 842–855
17. Kidoya H, Naito H, Takakura N: Apelin induces enlarged and nonleaky blood vessels for functional recovery from ischemia. Blood 2010, 115:3166–3174
18. Huang X, Yamada Y, Kidoya H, Naito H, Nagahama Y, Kong L, Katoh SY, Li WL, Ueno M, Takakura N: EphB4 overexpression in B16 melanoma cells affects arterial-venous patterning in tumor angiogenesis. Cancer Res 2007, 67:9800–9808
19. Nangia-Makker P, Honjo Y, Sarvis R, Akahani S, Hogan V, Pienta KJ, Raz A: Galectin-3 induces endothelial cell morphogenesis and angiogenesis. Am J Pathol 2000, 156:899–909
20. Hsu DK, Chernyavsky AI, Chen HY, Yu L, Grando SA, Liu FT: Endogenous galectin-3 is localized in membrane lipid rafts and regulates migration of dendritic cells. J Invest Dermatol 2009, 129: 573–583
21. Leek RD, Harris AL: Tumor-associated macrophages in breast cancer. J Mammary Gland Biol Neoplasia 2002, 7:177–189
22. Lin EY, Li JF, Bricard G, Wang W, Deng Y, Sellers R, Porcelli SA, Pollard JW: Vascular endothelial growth factor restores delayed tumor progression in tumors depleted of macrophages. Mol Oncol 2007, 1: 288–302
23. Giraudo E, Inoue M, Hanahan D: An amino-bisphosphonate targets MMP-9-expressing macrophages and angiogenesis to impair cervical carcinogenesis. J Clin Invest 2004, 114:623–633
24. Satoh T, Takeuchi O, Vandenbon A, Yasuda K, Tanaka Y, Kumagai Y, Miyake T, Matsushita K, Okazaki T, Saitoh T, Honma K, Matsuyama T, Yui K, Tsujimura T, Standley DM, Nakanishi K, Nakai K, Akira S: The Jmjd3-Irf4 axis regulates M2 macrophage polarization and host responses against helminth infection. Nat Immunol 2010, 11:936–944
25. Sica A, Allavena P, Mantovani A: Cancer related inflammation: the macrophage connection. Cancer Lett 2008, 267:204–215
26. Solinas G, Germano G, Mantovani A, Allavena P: Tumor-associated macrophages (TAM) as major players of the cancer-related inflammation. J Leukoc Biol 2009, 86:1065–1073
27. Noguera-Troise I, Daly C, Papadopoulos NJ, Coetzee S, Boland P, Gale NW, Lin HC, Yancopoulos GD, Thurston G: Blockade of Dll4 inhibits tumour growth by promoting non-productive angiogenesis. Nature 2006, 444:1032–1037
28. Nangia-Makker P, Balan V, Raz A: Regulation of tumor progression by extracellular galectin-3. Cancer Microenviron 2008, 1:43–51
29. Dagher SF, Wang JL, Patterson RJ: Identification of galectin-3 as a factor in pre-mRNA splicing. Proc Natl Acad Sci U S A 1995, 92: 1213–1217
30. Haudek KC, Spronk KJ, Voss PG, Patterson RJ, Wang JL, Arnoys EJ: Dynamics of galectin-3 in the nucleus and cytoplasm. Biochim Biophys Acta 2010, 1800:181–189
31. Califice S, Castronovo V, Van Den Brûle F: Galectin-3 and cancer (review). Int J Oncol 2004, 25:983–992
32. Perillo NL, Marcus ME, Baum LG: Galectins: versatile modulators of cell adhesion, cell proliferation, and cell death. J Mol Med 1998, 76: 402–412
33. Karlsson A, Christenson K, Matlak M, Björstad A, Brown KL, Telemo E, Salomonsson E, Leffler H, Bylund J: Galectin-3 functions as an opsonin and enhances the macrophage clearance of apoptotic neutrophils. Glycobiology 2009, 19:16–20
34. Frigeri LG, Liu FT: Surface expression of functional IgE binding protein, an endogenous lectin, on mast cells and macrophages. J Immunol 1992, 148:861–867
35. Liu FT, Frigeri LG, Gritzmacher CA, Hsu DK, Robertson MW, Zuberi RI: Expression and function of an IgE-binding animal lectin (epsilon BP) in mast cells. Immunopharmacology 1993, 26: 187–195
36. Allavena P, Mantovani A: Immunology in the clinic review series; focus on cancer: tumour-associated macrophages: undisputed stars of the inflammatory tumour microenvironment. Clin Exp Immunol 2012, 167:195–205
37. Mosser DM, Edwards JP: Exploring the full spectrum of macrophage activation. Nat Rev Immunol 2008, 8:958–969
38. Benoit M, Desnues B, Mege JL: Macrophage polarization in bacterial infections. J Immunol 2008, 181:3733–3739

39. Bronte V, Zanovello P: Regulation of immune responses by L-arginine metabolism. Nat Rev Immunol 2005, 5:641–654
40. Mantovani A, Sica A, Sozzani S, Allavena P, Vecchi A, Locati M: The chemokine system in diverse forms of macrophage activation and polarization. Trends Immunol 2004, 25:677–686
41. Stein M, Keshav S, Harris N, Gordon S: Interleukin 4 potently enhances murine macrophage mannose receptor activity: a marker of alternative immunologic macrophage activation. J Exp Med 1992, 176:287–292
42. Fidler IJ: Critical determinants of metastasis. Semin Cancer Biol 2002, 12:89–96
43. Takizawa H, Kondo K, Toba H, Kenzaki K, Sakiyama S, Tangoku A: Fluorescence diagnosis of lymph node metastasis of lung cancer in a mouse model. Oncol Rep 2009, 22:17–21
44. Markowska AI, Liu FT, Panjwani N: Galectin-3 is an important mediator of VEGF- and bFGF-mediated angiogenic response. J Exp Med 2010, 207:1981–1993
45. Legendre H, Decaestecker C, Nagy N, Hendlisz A, Schüring MP, Salmon I, Gabius HJ, Pector JC, Kiss R: Prognostic values of galectin-3 and the macrophage migration inhibitory factor (MIF) in human colorectal cancers. Mod Pathol 2003, 16:491–504

IJC
International Journal of Cancer

The novel phosphoinositide 3-kinase–mammalian target of rapamycin inhibitor, BEZ235, circumvents erlotinib resistance of *epidermal growth factor receptor* mutant lung cancer cells triggered by hepatocyte growth factor

Takako Sano[1], Shinji Takeuchi[1], Takayuki Nakagawa[1], Daisuke Ishikawa[1], Shigeki Nanjo[1], Tadaaki Yamada[1], Takahiro Nakamura[2], Kunio Matsumoto[2] and Seiji Yano[1]

[1] Division of Medical Oncology, Cancer Research Institute, Kanazawa University, Kanazawa, Japan
[2] Division of Tumor Dynamics and Regulation, Cancer Research Institute, Kanazawa University, Kanazawa, Japan

Acquired resistance to epidermal growth factor receptor–tyrosine kinase inhibitors (EGFR–TKIs), such as gefitinib and erlotinib, is a critical problem in the management of patients with *EGFR* mutant lung cancer. Several mechanisms have been reported involved in this acquired resistance, including hepatocyte growth factor (HGF) activation of an alternative pathway. PI3K and mTOR are downstream molecules of receptor tyrosine kinases, such as EGFR and Met, and are thought to be ideal targets for controlling various tumor types. We assessed whether BEZ235, a dual inhibitor of PI3K and mTOR, could overcome the EGFR–TKI resistance induced by HGF in an *EGFR* mutant lung cancer model. Exogenous and endogenous HGF triggered resistance to erlotinib in the PC-9 and HCC827, *EGFR* mutant lung cancer cell lines. BEZ235 alone inhibited the viability of PC-9 and HCC827 cells *in vitro*, irrespective of the presence or the absence of HGF. Using a xenograft model of severe combined immunodeficient mice with HGF-gene-transfected PC-9 cells (PC-9/HGF), we found that BEZ235 inhibited tumor growth, whereas erlotinib did not. BEZ235 monotherapy also inhibited the phosphorylation of Akt and p70S6K/S6RP, downstream molecules of PI3K and mTOR, respectively, as well as suppressing tumor-cell proliferation and angiogenesis of PC-9/HGF tumors. These results suggest that BEZ235, even as monotherapy, may be useful in managing HGF-induced EGFR–TKI resistance in *EGFR* mutant lung cancer.

Key words: HGF, EGFR-TKI resistance, PI3K, mTOR, *EGFR* mutation

Abbreviations: EGFR–TKI: epidermal growth factor receptor–tyrosine kinase inhibitor; HGF: hepatocyte growth factor; mTOR: mammalian target of rapamycin; PI3K: phosphoinositide 3-kinase; p70S6K: p70S6 kinase; S6RP: S6 ribosomal protein; VEGF: vascular endothelial growth factor

Additional Supporting Information may be found in the online version of this article.

Footnote: Conflict of Interest to be disclosed: S. Yano received honoraria from Chugai Pharmaceutical Co., Ltd. and AstraZeneca. S. Yano received research funding from Chugai Pharmaceutical Co., Ltd., Kyowa Hakko Kirin Co., Ltd. and Eisai Co., Ltd.

Grant sponsor: Grants-in-Aid of Cancer Research from the Ministry of Education, Science, Sports, and Culture of Japan; **Grand numbers:** 24390209; 22112010; 23790902; 11019957; **Grant sponsor:** P-Direct

DOI: 10.1002/ijc.28034

History: Received 27 Aug 2012; Accepted 27 Dec 2012; Online 15 Jan 2013

Correspondence to: Seiji Yano, Division of Medical, Oncology, Cancer Research Institute, Kanazawa University, 13-1 Takara-machi, Kanazawa, Ishikawa 920-0934, Japan, Fax: +81-76-234-4524, E-mail: syano@staff.kanazawa-u.ac.jp

Mutations activating epidermal growth factor receptor (EGFR), such as deletions of exon 19 and the L858R point mutation in exon 21, have been highly associated with clinical responses to the EGFR tyrosine kinase inhibitors (TKIs), gefitinib and erlotinib.[1–3] Almost all patients, however, develop acquired resistance to epidermal growth factor receptor tyrosine kinase inhibitors (EGFR–TKIs) after varying periods of time.[4] Thus, there is urgent need to develop effective therapies for these patients.

Recent studies have identified the molecular mechanisms of acquired resistance to EGFR–TKIs, including (*i*) gatekeeper mutations in *EGFR*, such as the T790M second mutation[5,6]; (*ii*) activation of bypass signaling caused by *Met* amplification,[7,8] hepatocyte growth factor (HGF) overexpression[9] or Gas6-Axl activation[10]; (*iii*) activation of downstream molecules (PTEN loss or PIK3CA mutation)[11,12]; (*iv*) small-cell lung cancer transformation[13] and (*v*) epithelial-to-mesenchymal transition.[14,15] We found that HGF overexpression triggers resistance by activating the Met/PI3K/Akt pathway,[9] a mechanism that may be involved in both intrinsic and acquired resistance to EGFR–TKIs.[9] For example, HGF overexpression was detected in 29 and 61% of tumor specimens from a Japanese cohort with *EGFR* mutant lung cancers and intrinsic and acquired resistance, respectively, to EGFR–TKIs.[16] Other studies have also reported a high frequency of

What's new?

Hepatocyte growth factor (HGF) activation of the alternative Met/PI3K/Akt signaling pathway is a common mechanism underlying the development of resistance to epidermal growth factor receptor (EGFR) tyrosine kinase inhibitors (TKIs) in EGFR mutant lung cancer. Here, the novel PI3K and mTOR dual inhibitor, BEZ235, was found to control the growth of tumor cells with HGF-mediated resistance to the TKI erlotinib both in vitro and in vivo. The results demonstrate BEZ235's potential for the management of HGF-induced TKI resistance in EGFR mutant lung cancer.

HGF overexpression in tumors with acquired resistance.[17,18] These findings indicate that management of HGF-triggered resistance is important for more successful treatment of patients with *EGFR* mutant lung cancer.

PI3K plays crucial roles in many cellular processes, including cell proliferation, survival, differentiation, motility and angiogenesis.[19–23] PI3K mediates signals from receptor tyrosine kinases, including EGFR and Met,[24] phosphorylating Akt and activating mTOR and downstream molecules, such as p70S6K and eukaryotic translation initiation factor 4E-binding protein 1, thereby regulating cell growth and gene transcription.[20–23,25,26] As activation of the PI3K pathway has been reported in various types of tumors, including *EGFR* mutant lung cancer,[19,21–24] PI3K and mTOR are also thought to be ideal therapeutic targets. We previously reported that PI3K inhibition with PI-103, a PI3K and mTOR inhibitor that will not enter clinical trials, resensitized *EGFR* mutant lung cancer cells to EGFR–TKI, even in the presence of HGF.[27] However, PI-103 monotherapy did not inhibit growth of EGFR–TKI-resistant tumors triggered by HGF, indicating the need to develop better PI3K inhibitors for clinical use.

BEZ235 is an orally available dual inhibitor of PI3K and mTOR that is being evaluated in phase I/II trials.[22,26,28] BEZ235 reversibly inhibits the catalytic activities of Class I PI3K and mTOR kinases by competitively inhibiting ATP binding.[28] We assessed whether BEZ235 can circumvent the EGFR–TKI resistance triggered by HGF in *EGFR* mutant lung cancer cells and we analyzed the mechanisms underlying its activity.

Material and Methods

Cell culture

The *EGFR* mutant human lung adenocarcinoma cell lines PC-9[29] and HCC827[7] were purchased from Immuno-Biological Laboratories (Takasaki, Gunma, Japan) and the American Type Culture Collection (ATCC; Manassas, VA), respectively. Human HGF-gene transfectant (PC-9/HGF) and vector control (PC-9/Vec) cells were established as described previously.[9] These cell lines were maintained in RPMI1640 medium supplemented with 10% fetal bovine serum (FBS), 100 units/mL penicillin, 100 units/mL streptomycin, and 2 mmol/L glutamine. All cells were passaged for <3 months before renewal from frozen, early-passage stocks. Cells were regularly screened for mycoplasma using a MycoAlert Mycoplasma Detection Kit (Lonza, Rockland, ME). These cell lines were authenticated at the laboratory of the National Institute of Biomedical Innovation (Osaka, Japan) by short-tandem repeat analysis. Human dermal microvessel endothelial cells (HMVECs) were maintained in HuMedia-MvG with growth supplements (purchased from Kurabo, Osaka, Japan in October 2012) and used for *in vitro* assay at passages 2–5.

Reagents

Erlotinib, BEZ235 and PI-103 were purchased from Selleck Chemicals, Houston, TX.

Cell viability assay

Cell viability was measured using the MTT [3-(4,5-dimethylthiazol-2-yl)-2,5-diphenyl tetrazolium] dye reduction method.[30] Tumor cells (2×10^3 cells/100 μL/well) in RPMI1640 medium with 10% FBS were plated into 96-well plates and cultured with indicated compounds for 72 hr, followed by the addition of 50 μL of MTT solution (2 mg/mL; Sigma, St. Louis, MO) to each well and further incubation for 2 hr. The medium was removed, and the dark blue crystals in each well were dissolved in 100 μL dimethyl sulfoxide. The absorbance of the wells was measured with a microplate reader at test and reference wavelengths of 550 and 630 nm, respectively. Percent growth was reported relative to untreated controls. Each experiment contained at least triplicate samples and was performed at least three times.

Antibodies and Western blotting

Cells were lysed in cell lysis buffer containing a phosphatase and proteinase inhibitor cocktail (Sigma, St. Louis, MO), and the protein concentrations were determined using a BCA Protein Assay Kit (Pierce Biotechnology, Rockford, IL). Total protein (40 μg) was resolved by SDS-polyacrylamide gel (Bio-Rad, Hercules, CA) electrophoresis and transferred to polyvinylidene difluoride membranes (Bio-Rad, Hercules, CA). After four washes, the membranes were incubated with Blocking One (Nacalai Tesque, Kyoto, Japan) for 1 hr at room temperature, followed by incubation overnight at 4°C with primary antibodies (Abs) to pEGFR (Y1068), pMet (Y1234/Y1235), Met (25H2), p-Akt (Ser473), Akt, p-p70S6K, p70S6K, p-S6RP and S6RP, each in 1:1000 dilution (Cell Signaling Technology, Danvers, MA); and primary Abs to human EGFR (1 μg/mL), p-ERK1/ERK2 and ERK1/ERK2, each diluted 1/1,000 (R&D Systems, Minneapolis, MN). After washing three times, the membranes were incubated for 1 hr

at room temperature with species-specific horseradish peroxidase-conjugated secondary Abs. Immunoreactive bands were visualized using SuperSignal West Dura Extended Duration Substrate Enhanced Chemiluminescent Substrate (Pierce Biotechnology, Rockford, IL). Each experiment was performed at least three times independently.

Xenografts in severe combined immunodeficient mice

Suspensions of PC-9/Vec and PC-9/HGF cells (3×10^6) were injected subcutaneously into the backs of 5-week-old female severe combined immunodeficient (SCID) mice (Clea, Tokyo, Japan). After 7 days, when the tumors were >5 mm in diameter, the mice were randomly allocated into groups of 6–10 each and treated with BEZ235 (20 mg/kg/day) and/or erlotinib (25 mg/kg/day) by oral gavage. Tumor volume was calculated daily, using the formula, volume (mm^3) = $width^2 \times length/2$). All animal experiments complied with the Guidelines for the Institute for Experimental Animals, Kanazawa University Advanced Science Research Center (Approval number: AP-081088).

Histological analyses

Proliferating cells were detected by incubating tissue sections with Ki-67 Ab (Clone MIB-1; DAKO, Glostrup, Denmark). Antigen was retrieved by microwaving tissue sections in 10 mM citrate buffer (pH = 6.0). After incubation with secondary Ab and treatment with the Vectastain ABC Kit (Vector Laboratories, Burlingame, CA), peroxidase activity was visualized using the diaminobenzidine (DAB) reaction. To analyze microvessel density, frozen sections (5 μm thick) of xenograft tumors were fixed with cold acetone and washed with PBS. After blocking endogenous peroxidase activity with 3% aqueous H_2O_2 solution for 10 min, the sections were incubated with 5% normal horse serum, washed and incubated overnight at 4°C with anti-mouse-CD31 (clone MEC13.3, BD Bioscience, San Jose, California) Ab. After washing with PBS, the sections were incubated with peroxidase-conjugated anti-

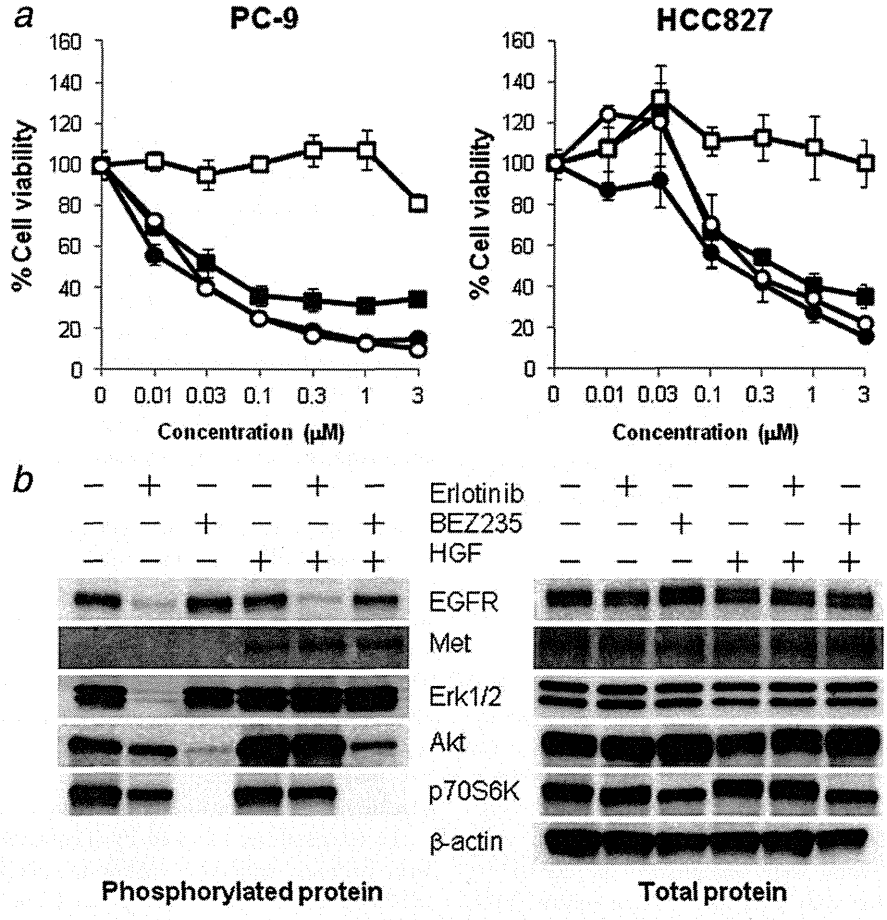

Figure 1. BEZ235 inhibited the viability of *EGFR* mutant lung cancer cells, irrespective of the presence of exogenous HGF. (*a*) PC-9 and HCC827 cells (2×10^3 cells/well) were incubated with various concentrations of drugs and/or HGF (20 ng/mL)(■: erlotinib, □: erlotinib + HGF, ●: BEZ235, ○: BEZ235 + HGF). Bars show standard deviation (SD). (*b*) PC-9 cells were treated with incubated with or without erlotinib (0.3 μM) or BEZ235 (0.3 μM) for 1 hr, followed by the addition of HGF (20 ng/mL) or PBS for 10 min. The cell lysates were harvested and subjected to Western blotting. The data shown are representative of three independent experiments with similar results.

rat IgG (Cell Signaling Technology, Danvers, MA) for 40 min. Peroxidase activity was visualized with DAB reactions. The sections were counterstained with hematoxylin.

Statistical analysis

Between-group differences were analyzed by one-way ANOVA. All statistical analyses were performed using GraphPad Prism Ver. 4.01 (GraphPad Software, San Diego, CA); $p < 0.05$ was considered statistically significant.

Results

BEZ235 suppressed the viability of *EGFR* mutant lung cancer cells in the presence of exogenous HGF

PC-9 and HCC827 cells were highly sensitive to erlotinib, whereas exogenously added HGF induced erlotinib resistance (Fig. 1*a*). BEZ235, a dual inhibitor of PI3K and mTOR, suppressed the viability of these cell lines in a dose-dependent manner. Under these experimental conditions, exogenously added HGF did not decrease the sensitivity of these cell lines to BEZ235, suggesting that BEZ235 may have the potential to overcome HGF-triggered resistance to EGFR-TKIs in *EGFR* mutant lung cancer cells.

BEZ235 suppressed the phosphorylation of Akt and its downstream molecules even in the presence of HGF

To explore the molecular mechanism by which BEZ235 suppressed cell viability, even in the presence of HGF, we examined the expression and phosphorylation status of the proteins EGFR and Met and their downstream molecules (Erk1/2, Akt and p70S6K) in PC-9 cells (Fig. 1*b*). In the absence of HGF, erlotinib inhibited the phosphorylation of EGFR and Erk1/2 markedly and Akt and p70S6K slightly. Although BEZ235 did not affect the phosphorylation of EGFR or Erk1/2, it markedly inhibited the phosphorylation of Akt and p70S6K. In the presence of HGF, erlotinib inhibited EGFR phosphorylation, but did not inhibit the phosphorylation of Met, Erk1/2, Akt and

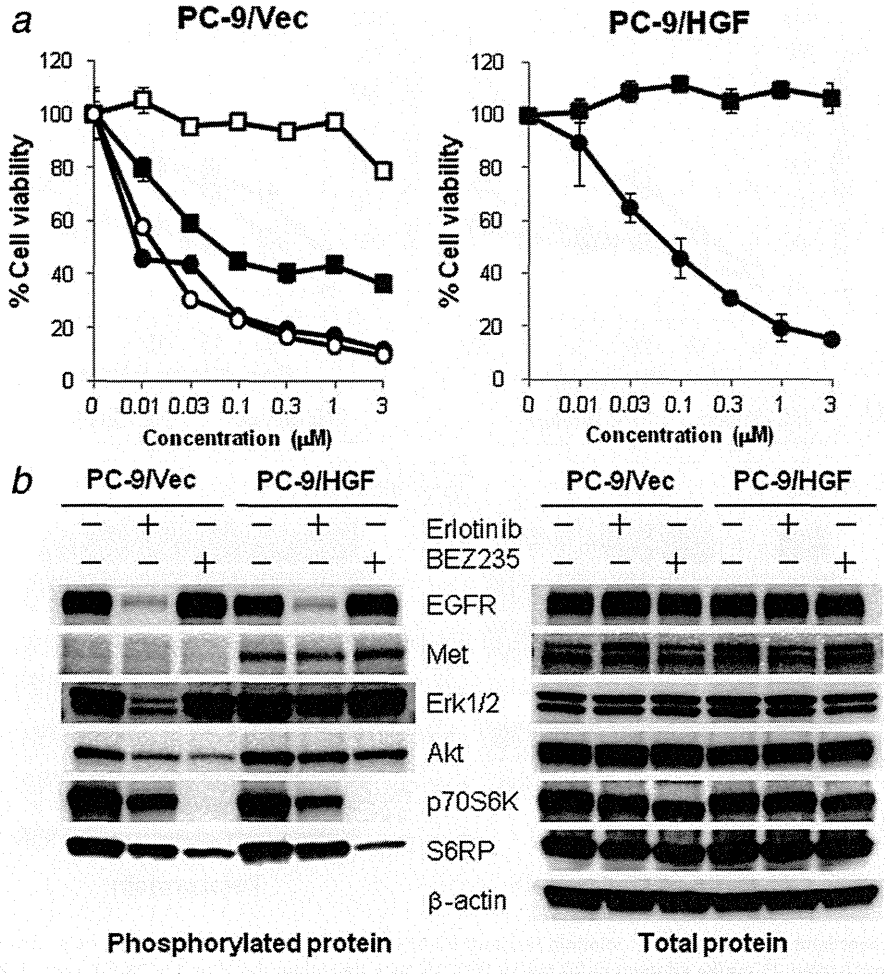

Figure 2. BEZ235 overcame erlotinib resistance caused by endogenous HGF. (*a*) PC-9/Vec and PC-9/HGF cells (2×10^3 cells/well) were incubated with various concentrations of drugs and/or HGF (20 ng/mL) (■: erlotinib, □: erlotinib + HGF, ●: BEZ235, ○:BEZ235 + HGF). Bars show SD. (*b*) PC-9/Vec and PC-9/HGF cells were treated with or without erlotinib (0.3 μM) or BEZ235 (0.3 μM) for 4 hr. The cell lysates were harvested and subjected to Western blotting. The data shown are representative of three independent experiments with similar results.

p70S6K. Although BEZ235 did not affect the phosphorylation of EGFR, Met or Erk1/2, it inhibited the phosphorylation of Akt and p70S6K. These results suggested that BEZ235 inhibited the viability of *EGFR* mutant lung cancer cells primarily by inhibiting the PI3K/mTOR (Akt/p70S6K) pathway, even in the presence of HGF.

BEZ235 suppressed the viability of *EGFR* mutant lung cancer cells in the presence of endogenous HGF

We previously showed that, in patients with *EGFR* mutant lung cancer and acquired resistance to EGFR–TKIs, HGF was present primarily in cancer cells, suggesting that autocrine HGF may be crucial roles for EGFR–TKI resistance in lung cancer patients.[31] To further explore the effect of BEZ235 on autocrine HGF-triggered resistance to EGFR–TKIs, we generated stable HGF-gene transfectants in PC-9 cells (PC-9/HGF); as a control, we generated PC-9 cells transfected with vector alone (PC-9/Vec). PC-9/HGF cells secreted high concentrations of HGF (27.8 ± 0.9 ng/48 hr), whereas the concentrations of HGF secreted by PC-9 and PC-9/Vec cells were under the limit of detection (data not shown). In addition, PC-9/HGF cells became resistant to erlotinib. We found that BEZ235 inhibited the viability of both PC-9/Vec and PC-9/HGF cells in a dose-dependent manner (Fig. 2*a*), whereas BEZ235 did not induce apoptosis (Supporting Information Fig. 1), in the line of the previous studies.[26] These results suggest that BEZ235 circumvented resistance induced by both endogenous and exogenous HGF.

We also examined the expression and phosphorylation status of the proteins EGFR, Met and their downstream

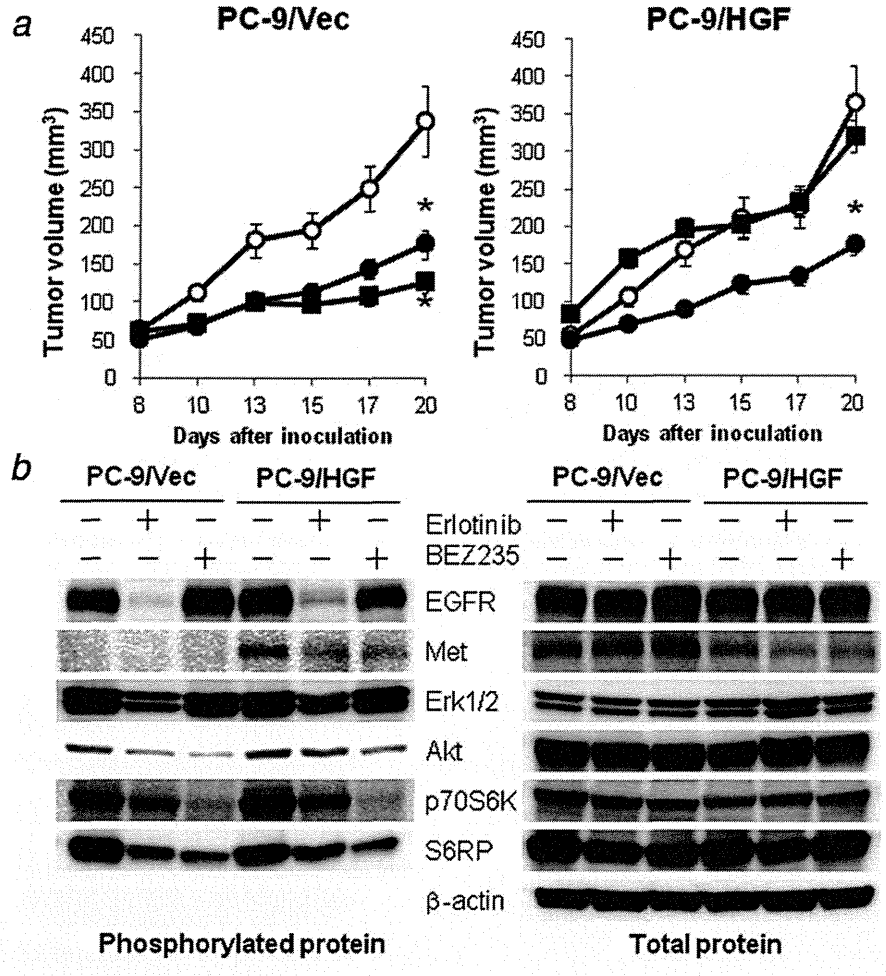

Figure 3. BEZ235 treatment inhibited the growth of erlotinib-resistant PC-9/HGF tumors in SCID mice. (*a*) SCID mice bearing PC-9/Vec or PC-9/HGF tumors were administered 25 mg/kg erlotinib or 20 mg/kg BEZ235 once daily from day 8 to day 20 (○: control, ■: erlotinib, ●: BEZ235). Tumor volume was measured using calipers on the indicated days. Mean ± SE tumor volumes are shown for groups of four to five mice. *$p < 0.01$ (one-way ANOVA). (*b*) SCID mice with PC-9/Vec or PC-9/HGF tumors were administered erlotinib 25 mg/kg and/or BEZ235 20 mg/kg daily for 4 days. Four hours after final administration, tumors were harvested and the relative levels of proteins in the tumor lysates were determined by Western blotting. The data shown are representative of two independent experiments with similar results.

molecules (Erk1/2, Akt and p70S6K) in PC-9/Vec and PC-9/HGF cells by Western blotting (Fig. 2*b*). PC-9/Vec cells expressed EGFR and Met proteins, with only EGFR being discernibly phosphorylated, as well as expressing the downstream proteins Erk1/2, Akt, p70S6K and S6RP, all of which were phosphorylated. Erlotinib inhibited the phosphorylation of EGFR, Erk1/2, Akt, p70S6K and S6RP. BEZ235 did not affect the phosphorylation of EGFR, Met or Erk1/2, but inhibited the phosphorylation of Akt slightly and p70S6K and S6RP, the downstream molecules of mTOR, markedly. In PC-9/HGF cells, Met was also phosphorylated presumably owing to HGF produced in an autocrine manner. Erlotinib inhibited the phosphorylation of EGFR, but not of Met, Erk1/2, Akt or p70S6K. In contrast, BEZ235 did not inhibit the phosphorylation of EGFR, Met or Erk1/2, but inhibited the phosphorylation of Akt slightly and p70S6K and S6RP markedly. These results indicate that BEZ235 suppresses the phosphorylation of downstream molecules of mTOR, irrespective of the presence or the absence of endogenous HGF.

BEZ235 suppressed the growth of erlotinib-resistant tumors induced by HGF *in vivo*

We next evaluated whether BEZ235 could overcome HGF-induced resistance to erlotinib *in vivo*. Oral administration of erlotinib or BEZ235 markedly suppressed the growth of PC-9/Vec tumors (Fig. 3*a*). In contrast, erlotinib failed to inhibit the growth of PC-9/HGF-tumors, indicating that HGF induced resistance to erlotinib *in vivo*. Under these experimental conditions, BEZ235 markedly suppressed the growth of PC-9/HGF tumors, indicating that BEZ235 may be useful for controlling the growth of HGF-induced erlotinib-resistant tumors. We also assessed the molecular mechanisms by which BEZ235 inhibited the growth of PC-9/HGF tumors. Western

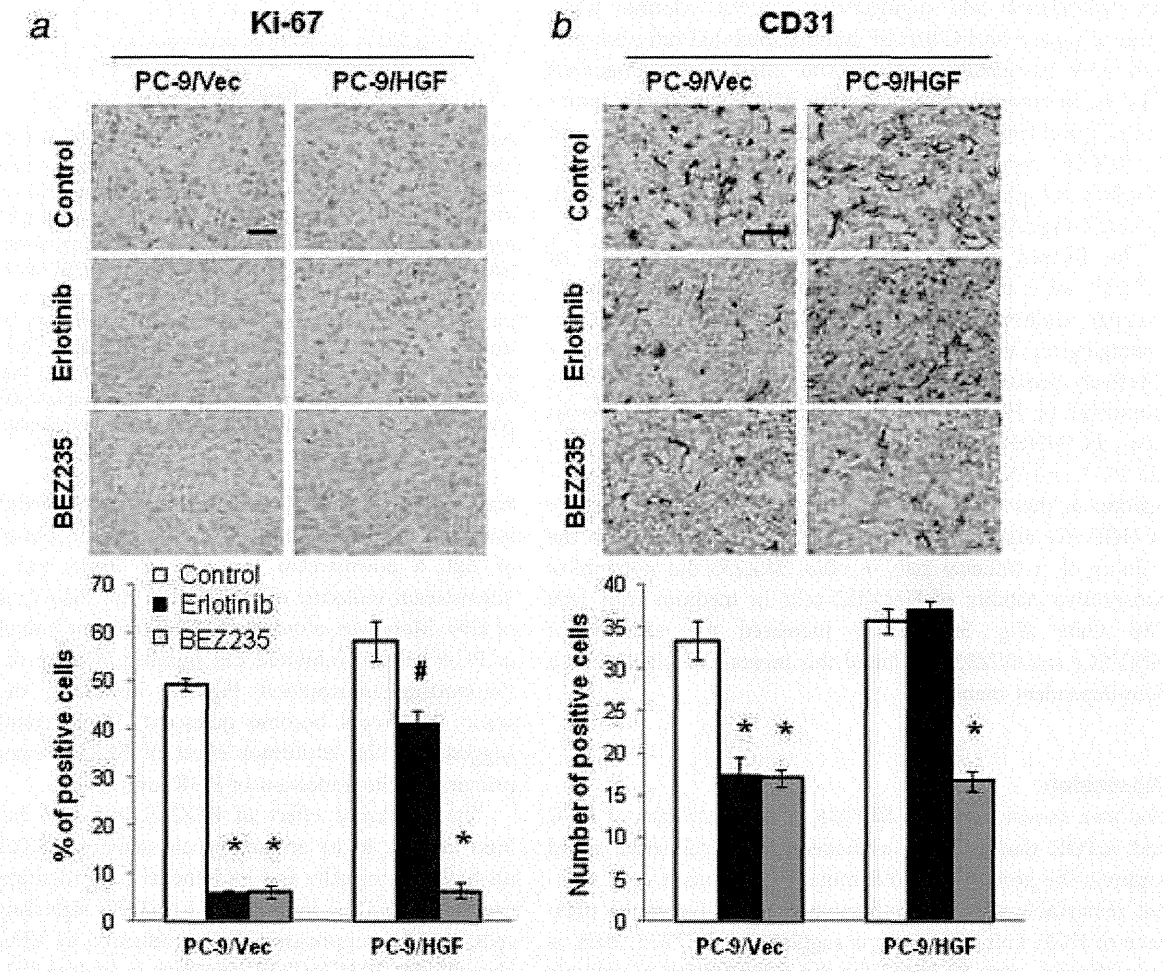

Figure 4. BEZ235 treatment inhibited tumor-cell proliferation and angiogenesis. SCID mice with PC-9/Vec or PC-9/HGF tumors were administered erlotinib 25 mg/kg and/or BEZ235 20 mg/kg daily for 4 days. Four hours after final administration, tumors were harvested and tumor cell proliferation (*a*: Ki-67, bar: 50 μm) and angiogenesis (*b*: CD31, bar: 100 μm) were determined by immunohistochemistry. Lower panes show quantification of positive cells. $^{\#}p < 0.01$, $^{*}p < 0.001$ (one-way ANOVA). Bars show standard errors. The data shown are representative of two independent experiments with similar results. [Color figure can be viewed in the online issue, which is available at wileyonlinelibrary.com.]

blot analyses showed that erlotinib markedly inhibited the phosphorylation of EGFR and Erk1/2 and slightly inhibited the phosphorylation of Akt and p70S6K in PC-9/Vec tumors (Fig. 3*b*). In PC-9/HGF tumors, Met was phosphorylated, whereas erlotinib markedly inhibited the phosphorylation of EGFR and slightly inhibited the phosphorylation of Met, Erk1/2, Akt and p70S6K. Although BEZ235 had no effect on the phosphorylation of EGFR or Erk1/2, it markedly inhibited the phosphorylation of Akt and p70S6K. These results indicated that the antitumor effects of BEZ235 on the growth of PC-9/HGF cells may be owing primarily to its inhibition of the PI3K/mTOR (Akt/p70S6K) pathway.

We also examined tumor cell proliferation (Ki-67), apoptosis (TUNEL) and angiogenesis (CD31) by immunohistochemistry. Although erlotinib treatment induced apoptosis in PC-9/Vec tumors but not PC-9/HGF tumors, BEZ235 treatment did not induce apoptosis in PC-9/Vec or PC-9/HGF tumors (Supporting Information Fig. 2). Erlotinib treatment of animals with PC-9/Vec tumors markedly inhibited tumor cell proliferation and angiogenesis, whereas erlotinib treatment of mice with PC-9/HGF tumors inhibited cell proliferation only marginally and had no effect on angiogenesis (Fig. 4). In contrast, treatment with BEZ235 markedly inhibited cell proliferation and angiogenesis of both PC-9/Vec and PC-9/HGF tumors. These findings suggest that BEZ235 inhibited the growth of PC-9/HGF tumors, at least in part, by inhibiting angiogenesis.

To further explore the antiangiogenic influence of BEZ235, we examined its effect on tumor cell production of vascular endothelial growth factor (VEGF), a prominent proangiogenic molecule. Both PC-9 and PC-9/Vec cells constitutively produced detectable levels of VEGF, which were stimulated by HGF (Fig. 5*a*). Consistent with these observations, PC-9/HGF cells produced higher levels of VEGF than did PC-9 and PC-9/Vec cells. BEZ235 suppressed VEGF production in these cancer cells in the presence or the absence of HGF. We also assessed the direct effect of BEZ235 on the viability of endothelial cells *in vitro*. BEZ235 did not inhibit constitutive viability of HMVEC cells in medium with 10% FBS alone (Fig. 5*b*). VEGF increased the viability of HMVECs and BEZ235 inhibited this increase in viability in a dose-dependent manner.

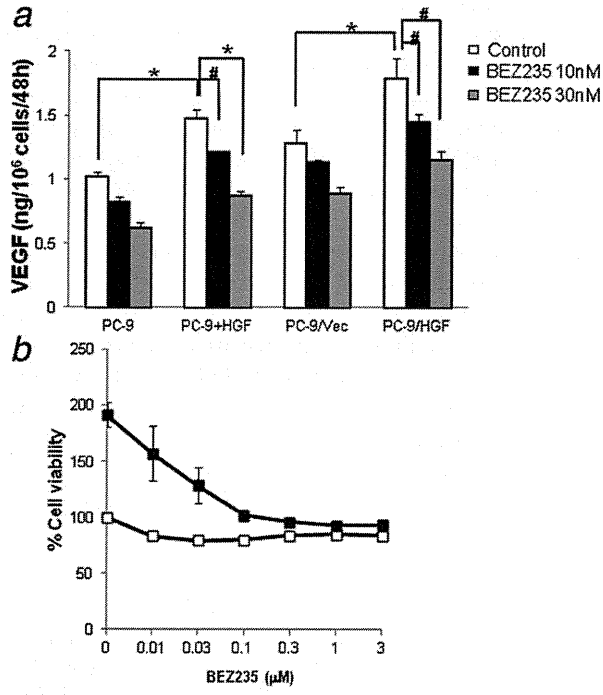

Figure 5. BEZ235 inhibited VEGF production by cancer cells and endothelial viability. (*a*) Tumor cells were incubated with or without HGF (50 ng/mL) in the presence of different concentrations of BEZ235 for 48 hr. Then, supernatants were harvested and the number of tumor cells was counted. VEGF concentration in the supernatants was determined by ELISA (R&D Systems). VEGF levels corrected for tumor cell number are shown. $^{\#}p < 0.05$, $^{*}p < 0.001$. (*b*) HMVECs were incubated in RPMI-1640 medium with 10% FBS (control), or RPMI-1640 medium with 10% FBS plus VEGF (50 ng/mL) with different concentrations of BEZ235 for 72 hr. Then, cell viability was determined using the MTT assay. Bars show SD. The data shown are from two independent experiments with similar results.

Discussion

We have shown here that BEZ235, a dual inhibitor of PI3K and mTOR that is being evaluated in clinical trials, could suppress the growth of *EGFR* mutant lung cancer cells without remarkable apoptosis induction, irrespective of the presence of HGF. Our observations suggest that BEZ235, even as monotherapy, may be useful for the management of patients with *EGFR* mutant lung cancer and HGF-induced EGFR-TKI resistance.

Activation of the PI3K/Akt and mitogen-activated protein kinase/Erk pathways has been shown crucial for the survival and growth of *EGFR* mutant lung cancer cells.[29,32,33] We found that BEZ235 markedly inhibited the phosphorylation of Akt, a downstream molecule of PI3K, and p70S6K, a downstream molecule of mTOR, but not Erk1/2, *in vitro* and *in vivo*. Moreover, although BEZ235 did not induce apoptosis of PC-9 cells, it inhibited cell number increase of PC-9 cells (Supporting Information Fig. 3), indicating that BEZ235 made PC-9 cells become quiescent. These results strongly suggest that the antitumor effect of BEZ235 may be owing primarily to its inhibition of PI3K and mTOR.

The antitumor effect of BEZ235 may also be owing, at least in part, to its antiangiogenic activity. BEZ235 may act on both cancer cells and endothelial cells to suppress angiogenesis.[34] BEZ235 inhibits PI3K/mTOR signaling in tumor cells, thereby suppressing their production of VEGF. BEZ235 also inhibits PI3K/mTOR signaling in endothelial cells, suppressing their proliferation and permeability.[35] We recently reported that HGF activates the Met/PI3K/Akt pathway and facilitates not only EGFR-TKI resistance but also angiogenesis *via* VEGF production in *EGFR* mutant lung cancer cells.

Our findings here confirm these observations and further demonstrate that BEZ235 markedly inhibited angiogenesis in an *in vivo* model of HGF-producing *EGFR* mutant lung tumors resistant to the EGFR-TKI erlotinib. Collectively, these findings suggest that BEZ235 may have the potential to control the progression of *EGFR* mutant lung cancers *via* multiple mechanisms, including the inhibition of the resistance signal to EGFR-TKI and the suppression of angiogenesis.

Several PI3K inhibitors have been developed and are being evaluated in clinical trials against various types of tumors. PI-103 is a dual PI3K and mTOR inhibitor that revealed favorable antitumor activity *in vitro* and *in vivo*.[36] We previously reported that the combination of PI-103 and gefitinib strongly suppressed Akt phosphorylation and circumvented HGF-triggered gefitinib resistance in an *in vivo* model of *EGFR* mutant lung cancer, whereas PI-103 alone had no activity. We have shown here that BEZ235 alone markedly inhibited the growth of HGF-producing, erlotinib-resistant *EGFR* mutant lung cancer tumors *in vivo*, indicating that this agent may have a higher potential relative to PI-103 as monotherapy. There are at least explanations for the superior activity of BEZ235 relative to PI-103. First, the two agents differ in anti-mTOR activity although both have similar IC_{50}s for PI3Ks.[26,28,37] In our experiments with HGF-gene transfectants, a PI-103 concentration of >0.3 μM was required to discernibly inhibit the phosphorylation of p70S6K, a downstream molecule of mTOR, whereas much lower concentrations of BEZ235 were required (Supporting Information Fig. 4A). Similarly, 0.3 μM BEZ235 was more effective than 1 μM PI-103 in terms of inhibition of PC-9-cell viability (Supporting Information Fig. 4B). Recent studies also reported that the concentration of BEZ235 required to inhibit the growth of breast cancer cell lines with a *KRAS* or *PIK3CA* mutation was about 100-fold lower than the concentration of PI-103.[38] Moreover, the addition of the mTOR inhibitor rapamycin to PI-103 markedly inhibited Akt-Ser473 phosphorylation, thereby suppressing cell growth.[39] We also found that the single use of GDC-0941 (a selective PI3K inhibitor) or rapamycin inhibited the viability of PC-9 cells by about 40% and their combined use further inhibited cell viability, irrespective of the presence of HGF. Moreover, combined use of rapamycin and PI-103 also further inhibited cell viability, just like BEZ235 alone (Supporting Information Fig. 4B). These results indicate the importance of the combined inhibition of PI3K and mTOR. The second reason for the difference between BEZ235 and PI-103 may be owing to the differences in drug metabolism and pharmacodynamics. PI-103 is rapidly metabolized in cells, with a half life of 0.7–1.3 hr,[37] whereas BEZ235 potently inhibited Akt-Ser473 as late as 16 hr after *in vivo* administration.[28] Therefore, BEZ235 may inhibit target activity in tumor cells more durably than PI-103, and may thereby be more effective than PI-103.

BEZ235 is being evaluated in clinical trials in various types of tumors, including lung cancer. Several trials have shown the safety of this compound when given as monotherapy. When 400 mg of BEZ235 was given twice daily (800 mg/day) in solid tumors, Cmax reached more than 7,000,ng/mL.[40] Therefore, the doses of BEZ235 we used in our study seem to be clinically relevant and the findings presented here suggest that BEZ235 may control *EGFR* mutant lung cancer even after they develop resistance to EGFR-TKIs. Clinical evaluation of BEZ235 in patients with EGFR-TKI-resistant *EGFR* mutant lung cancer is warranted.

Acknowledgements

Our study was supported by Grants-in-Aid of Cancer Research from the Ministry of Education, Science, Sports, and Culture of Japan (S. Yano, 24390209 and 22112010; T. Yamada, 23790902 and S. Takeuchi, 11019957) and P-Direct. The authors thank Mr. Kenji Kita for technical assistance.

References

1. Lynch TJ, Bell DW, Sordella R, et al. Activating mutations in the epidermal growth factor receptor underlying responsiveness of non-small-cell lung cancer to gefitinib. *N Engl J Med* 2004;350:2129–39.
2. Paez JG, Jänne PA, Lee JC, et al. EGFR mutations in lung cancer: correlation with clinical response to gefitinib therapy. *Science* 2004;304:1497–500.
3. Pao W, Miller V, Zakowski M, et al. EGF receptor gene mutations are common in lung cancers from "never smokers" and are associated with sensitivity of tumors to gefitinib and erlotinib. *Proc Natl Acad Sci USA* 2004;101:13306–11.
4. Jackman D, Pao W, Riely GJ, et al. Clinical definition of acquired resistance to epidermal growth factor receptor tyrosine kinase inhibitors in non-small-cell lung cancer. *J Clin Oncol* 2010;28:357–60.
5. Kobayashi S, Boggon TJ, Dayaram T, et al. EGFR mutation and resistance of non-small-cell lung cancer to gefitinib. *N Engl J Med* 2005;352:786–92.
6. Pao W, Miller VA, Politi KA, et al. Acquired resistance of lung adenocarcinomas to gefitinib or erlotinib is associated with a second mutation in the EGFR kinase domain. *PLoS Med* 2005;2:e73.
7. Engelman JA, Zejnullahu K, Mitsudomi T, et al. MET amplification leads to gefitinib resistance in lung cancer by activating ERBB3 signaling. *Science* 2007;316:1039–43.
8. Bean J, Brennan C, Shih JY, et al. MET amplification occurs with or without T790M mutations in EGFR mutant lung tumors with acquired resistance to gefitinib or erlotinib. *Proc Natl Acad Sci USA* 2007;104:20932–7.
9. Yano S, Wang W, Li Q, et al. Hepatocyte growth factor induces gefitinib resistance of lung adenocarcinoma with epidermal growth factor receptor-activating mutations. *Cancer Res* 2008;68:9479–87.
10. Zhang Z, Lee JC, Lin L, et al. Activation of the AXL kinase causes resistance to EGFR-targeted therapy in lung cancer. *Nat Genet* 2012;44:852–60.
11. Ludovini V, Bianconi F, Pistola L, et al. Phosphoinositide-3-kinase catalytic alpha and KRAS mutations are important predictors of resistance to therapy with epidermal growth factor receptor tyrosine kinase inhibitors in patients with advanced non-small cell lung cancer. *J Thorac Oncol* 2011;6:707–15.
12. Yamamoto C, Basaki Y, Kawahara A, et al. Loss of PTEN expression by blocking nuclear translocation of EGR1 in gefitinib-resistant lung cancer cells harboring epidermal growth factor receptor-activating mutations. *Cancer Res* 2010;70:8715–25.
13. Sequist LV, Waltman BA, Dias-Santagata D, et al. Genotypic and histological evolution of lung cancers acquiring resistance to EGFR inhibitors. *Sci Transl Med* 2011;3:75ra26.
14. Suda K, Tomizawa K, Fujii M, et al. Epithelial to mesenchymal transition in an epidermal growth factor receptor-mutant lung cancer cell line with

acquired resistance to erlotinib. *J Thorac Oncol* 2011;6:1152–61.
15. Uramoto H, Shimokawa H, Hanagiri T, et al. Expression of selected gene for acquired drug resistance to EGFR-TKI in lung adenocarcinoma. *Lung Cancer* 2011;73:361–5.
16. Yano S, Yamada T, Takeuchi S, et al. Hepatocyte growth factor expression in EGFR mutant lung cancer with intrinsic and acquired resistance to tyrosine kinase inhibitors in a Japanese cohort. *J Thorac Oncol* 2011;6:2011–7.
17. Turke AB, Zejnullahu K, Wu YL, et al. Preexistence and clonal selection of MET amplification in EGFR mutant NSCLC. *Cancer Cell* 2010;17:77–88.
18. Onitsuka T, Uramoto H, Nose N, et al. Acquired resistance to gefitinib: the contribution of mechanisms other than the T790M, MET, and HGF status. *Lung Cancer* 2010;68:198–203.
19. Vivanco I, Sawyers CL. The phosphatidylinositol 3-Kinase AKT pathway in human cancer. *Nat Rev Cancer* 2002;2:489–501.
20. Bader AG, Kang S, Zhao L, et al. Oncogenic PI3K deregulates transcription and translation. *Nat Rev Cancer* 2005;5:921–9.
21. Engelman JA, Luo J, Cantley LC. The evolution of phosphatidylinositol 3-kinases as regulators of growth and metabolism. *Nat Rev Genet* 2006;7:606–19.
22. Liu P, Cheng H, Roberts TM, et al. Targeting the phosphoinositide 3-kinase pathway in cancer. *Nat Rev Drug Discov* 2009;8:627–44.
23. Courtney KD, Corcoran RB, Engelman JA. The PI3K pathway as drug target in human cancer. *J Clin Oncol* 2010;28:1075–83.
24. Engelman JA. Targeting PI3K signalling in cancer: opportunities, challenges and limitations. *Nat Rev Cancer* 2009;9:550–62.
25. Bjornsti MA, Houghton PJ. The TOR pathway: a target for cancer therapy. *Nat Rev Cancer* 2004;4:335–48.
26. Guertin DA, Sabatini DM. The pharmacology of mTOR inhibition. *Sci Signal* 2009;2:pe24.
27. Donev IS, Wang W, Yamada T, et al. Transient PI3K inhibition induces apoptosis and overcomes HGF-mediated resistance to EGFR-TKIs in EGFR mutant lung cancer. *Clin Cancer Res* 2011;17:2260–9.
28. Maira SM, Stauffer F, Brueggen J, et al. Identification and characterization of NVP-BEZ235, a new orally available dual phosphatidylinositol 3-kinase/mammalian target of rapamycin inhibitor with potent in vivo antitumor activity. *Mol Cancer Ther* 2008;7:1851–63.
29. Ono M, Hirata A, Kometani T, et al. Sensitivity to gefitinib (Iressa, ZD1839) in non-small cell lung cancer cell lines correlates with dependence on the epidermal growth factor (EGF) receptor/extracellular signal-regulated kinase 1/2 and EGF receptor/Akt pathway for proliferation. *Mol Cancer Ther* 2004;3:465–72.
30. Green LM, Reade JL, Ware CF. Rapid colorimetric assay for cell viability: application to the quantitation of cytotoxic and growth inhibitory lymphokines. *J Immunol Methods* 1984;70:257–68.
31. Wang W, Li Q, Yamada T, et al. Crosstalk to stromal fibroblasts induces resistance of lung cancer to epidermal growth factor receptor tyrosine kinase inhibitors. *Clin Cancer Res* 2009;15:6630–8.
32. Engelman JA, Jänne PA, Mermel C, et al. ErbB-3 mediates phosphoinositide 3-kinase activity in gefitinib-sensitive non-small cell lung cancer cell lines. *Proc Natl Acad Sci USA* 2005;102:3788–93.
33. Faber AC, Li D, Song Y, et al. Differential induction of apoptosis in HER2 and EGFR addicted cancers following PI3K inhibition. *Proc Natl Acad Sci USA* 2009;106:19503–8.
34. Liu TJ, Koul D, LaFortune T, et al. NVP-BEZ235, a novel dual phosphatidylinositol 3-kinase/mammalian target of rapamycin inhibitor, elicits multifaceted antitumor activities in human gliomas. *Mol Cancer Ther* 2009;8:2204–10.
35. Schnell CR, Stauffer F, Allegrini PR, et al. Effects of the dual phosphatidylinositol 3-kinase/mammalian target of rapamycin inhibitor NVP-BEZ235 on the tumor vasculature: implications for clinical imaging. *Cancer Res* 2008;68:6598–607.
36. Kong D, Yamori T. Phosphatidylinositol 3-kinase inhibitors: promising drug candidates for cancer therapy. *Cancer Sci* 2008;99:1734–40.
37. Raynaud FI, Eccles S, Clarke PA, et al. Pharmacologic characterization of a potent inhibitor of class I phosphatidylinositide 3-kinases. *Cancer Res* 2007;67:5840–50.
38. Brachmann SM, Hofmann I, Schnell C, et al. Specific apoptosis induction by the dual PI3K/mTor inhibitor NVP-BEZ235 in HER2 amplified and PIK3CA mutant breast cancer cells. *Proc Natl Acad Sci USA* 2009;106:22299–304.
39. Mazzoletti M, Bortolin F, Brunelli L, et al. Combination of PI3K/mTOR inhibitors: antitumor activity and molecular correlates. *Cancer Res* 2011;71:4573–84.
40. Arkenau HT, Jones SF, Kurkjian C, et al. The PI3K/mTOR inhibitor BEZ235 given twice daily for the treatment of patients (pts) with advanced solid tumors. *J Clin Oncol* 2012;30: abstr 3097.

Oncogene (2012), 1–9

www.nature.com/onc

ORIGINAL ARTICLE

Akt kinase-interacting protein1, a novel therapeutic target for lung cancer with *EGFR*-activating and gatekeeper mutations

T Yamada[1], S Takeuchi[1], N Fujita[2], A Nakamura[2], W Wang[1], Q Li[1], M Oda[3], T Mitsudomi[4], Y Yatabe[5], Y Sekido[6], J Yoshida[7], M Higashiyama[8], M Noguchi[9], H Uehara[10], Y Nishioka[11], S Sone[11] and S Yano[1]

Despite initial dramatic response, epidermal growth factor receptor (EGFR) mutant lung cancer patients always acquire resistance to EGFR-tyrosine kinase inhibitors (TKIs). Gatekeeper T790M mutation in *EGFR* is the most prevalent genetic alteration underlying acquired resistance to EGFR-TKI, and *EGFR* mutant lung cancer cells are reported to be addictive to EGFR/Akt signaling even after acquired T790M mutation. Here, we focused on Akt kinase-interacting protein1 (Aki1), a scaffold protein of PI3K (phosphoinositide 3-kinase)/PDK1 (3-phosphoinositide-dependent protein kinase)/Akt that determines receptor signal selectivity for non-mutated *EGFR*, and assessed its role in *EGFR* mutant lung cancer with or without gatekeeper T790M mutation. Cell line-based assays showed that Aki1 constitutively associates with mutant *EGFR* in lung cancer cells with (H1975) or without (PC-9 and HCC827) T790M gatekeeper mutation. Silencing of *Aki1* induced apoptosis of *EGFR* mutant lung cancer cells. Treatment with *Aki1* siRNA dramatically inhibited growth of H1975 cells in a xenograft model. Moreover, silencing of *Aki1* further potentiated growth inhibitory effect of new generation EGFR-TKIs against H1975 cells *in vitro*. Aki1 was frequently expressed in tumor cells of *EGFR* mutant lung cancer patients (53/56 cases), including those with acquired resistance to EGFR-TKI treatment (7/7 cases). Our data suggest that Aki1 may be a critical mediator of survival signaling from mutant *EGFR* to Akt, and may therefore be an ideal target for *EGFR* mutant lung cancer patients, especially those with acquired EGFR-TKI resistance due to *EGFR* T790M gatekeeper mutation.

Oncogene advance online publication, 8 October 2012; doi:10.1038/onc.2012.446

Keywords: Akt kinase-interacting protein1; *EGFR* mutation; novel therapeutic target; lung cancer

INTRODUCTION

Lung cancer with epidermal growth factor receptor (EGFR)-activating mutations, such as exon 19 deletion and exon 21 L858R point mutation, responds to the EGFR-tyrosine kinase inhibitors (EGFR-TKIs) gefitinib and erlotinib.[1] Recent clinical trials demonstrated much longer progression-free survival for EGFR mutant lung cancer patients when treated with gefitinib compared with conventional chemotherapy.[2,3] However, almost without exception, the responders relapse after various times due to acquiring resistance to EGFR-TKIs.[1,4]

The development of gatekeeper mutations, such as T315I in Abl,[5] D473H in SMO[6] and L1196M in ALK,[7] is the most common mechanism of acquired TKI resistance.[8] In cases of *EGFR* mutant lung cancer, *EGFR* T790M mutation is detected in about 50% of patients with acquired resistance to EGFR-TKIs.[4,8,9] T790M mutation results in increased EGFR affinity to adenosine triphosphate, reducing binding of EGFR-TKIs, and thus inducing resistance.[10] However, *EGFR* mutant lung cancer cells with T790M mutation are still dependent on EGFR-mediated signaling,[10] and therefore further elucidation of mutant EGFR-mediated signaling may facilitate the development of novel effective therapeutic strategies against lung cancer with *EGFR* mutations, including T790M gatekeeper mutation.

New generation EGFR-TKIs, such as irreversible EGFR-TKIs and mutant EGFR selective TKIs, were expected to overcome acquired resistance caused by T790M secondary mutation.[11–15] However, several irreversible EGFR-TKIs failed to meet primary end points in clinical trials in EGFR-TKI-refractory lung cancer and induced severe adverse effects, such as diarrhea, skin rush/acne, stomatitis and nail effect.[1,16] More recently, a phase Ib trial of EGFR dual inhibition with irreversible EGFR-TKI afatinib plus anti-EGFR monoclonal antibody cetuximab indicated with a 40% objective response rate in 47 patients with EGFR-TKI acquired resistance,[17] suggesting that many tumors are still addicted to the EGFR signaling pathway, including *EGFR* T790M gatekeeper mutation in clinical trials. Therefore, new intensification treatment targeting EGFR signaling is expected to get for more clinical benefit, whereas the feasibility of these strategies should be evaluated carefully in clinical trials.

Receptor tyrosine kinases, such as EGFR, PDGFRs and VEGFRs, utilize several common downstream signaling pathways, including MAPK/ERK and PI3K/Akt, while each receptor shows different or specific biological activity after ligand stimulation. Scaffold proteins that can simultaneously interact with two or more protein binding partners are thought to ensure specificity as well as temporal regulation of signal transduction. Thus, scaffold

[1]Division of Medical Oncology, Cancer Research Institute, Kanazawa University, Kanazawa, Japan; [2]Cancer Chemotherapy Center, Japanese Foundation for Cancer Research, Tokyo, Japan; [3]Department of General and Cardiothoracic Surgery, Kanazawa University, Kanazawa, Japan; [4]Department of Thoracic Surgery, Aichi Cancer Center Hospital, Nagoya, Japan; [5]Department of Pathology, Aichi Cancer Center Hospital, Nagoya, Japan; [6]Division of Molecular Oncology, Aichi Cancer Center Research Institute, Nagoya, Japan; [7]Department of Thoracic Oncology, National Cancer Center Hospital East, Kashiwa, Japan; [8]Department of Thoracic Surgery, Osaka Medical Center for Cancer and Cardiovascular Diseases, Osaka, Japan; [9]Department of Pathology, Institute of Basic Medical Sciences, University of Tsukuba, Tsukuba, Japan; [10]Department of Molecular and Environmental Pathology, Institute of Health Biosciences, The University of Tokushima Graduate School, Tokushima, Japan and [11]Department of Respiratory Medicine & Rheumatology, Institute of Health Biosciences, The University of Tokushima Graduate School, Tokushima, Japan. Correspondence: Dr T Yamada, Division of Medical Oncology, Cancer Research Institute, Kanazawa University, Takara-machi 13-1, Kanazawa, Ishikawa 920-0934, Japan.
E-mail: tadaakiy@med.kanazawa-u.ac.jp
Received 9 April 2012; revised 7 August 2012; accepted 9 August 2012

proteins may be important targets for regulating receptor-mediated signaling. There is accumulating evidence that Akt signaling is essential for mediating survival signals in *EGFR* mutant lung cancer cells.[18,19] Although several molecules, including KSP,[20] Paxillin,[21] RKIP,[22] and JIP-1,[23] are known to act as scaffolds for MAPK-ERK,[24] scaffold proteins for Akt have not been well documented. Recently, we reported Akt kinase-interacting protein1 (Aki1) as the first identified scaffold in the PI3K/PDK1/Akt pathway. Aki1 selectively forms a complex with EGFR and Akt in response to EGF stimulation, mediates Akt activation by PDK1, and hence contributes to cell survival and proliferation.[25] However, Aki1, the scaffold proteins for therapeutic target in cancers, have yet to be identified.

In the present study, we examined whether Aki1 would act as a determinant of receptor signaling selectivity of mutant EGFR and could be a therapeutic target for *EGFR* mutant lung cancer, including that with T790M gatekeeper mutation.

RESULTS

High levels of Aki1 protein expression in *EGFR* mutant lung cancer cell lines

As the first step to assess the involvement of Aki1 in EGFR-mediating signal of lung cancer cells, we examined the expression of Aki1 protein and its associated proteins (PDK1, Akt and EGFR) in five human lung adenocarcinoma cells with or without *EGFR* mutations, comparing that in two human lung embryonic fibroblast cell lines, by western blotting (Figure 1a). All of the cell lines examined expressed Aki1 and PDK1 protein at various levels. The levels of Aki1 tend to be higher in EGFR mutant lung cancer cell lines than in lung fibroblast cell lines.

EGFR was also detected in all lung cancer and fibroblast cell lines at various levels. Interestingly, phosphorylated EGFR was detected in EGFR mutant lung cancer cell lines, but not detected in EGFR wild-type lung cancer cell lines and fibroblast cell lines. The co-detection of Aki1 and phosphorylated EGFR in these cell lines suggested interactions between Aki1 and mutant EGFR because Aki1 was shown to bind preferentially to activated wild-type EGFR.[25]

Aki1 constitutively associates with *EGFR* without ligand stimulation in *EGFR* mutant lung cancer cells

To determine the role of Aki1 in the EGFR/PDK1/Akt pathway, we examined the association between Aki1 and EGFR by immunoprecipitation. Aki1 constitutively associated with EGFR in all three *EGFR* mutant lung cancer cell lines (Figure 1b). Consistent with the results of previous studies,[25] Aki1 did not associate with IGF-1 R, irrespective of IGF-1 stimulation, indicating selective binding of Aki1 to EGFR (Figure 1b). Moreover, treatment with EGFR-TKI did not affect the association between Aki1 and EGFR/PDK1/Akt (Supplementary Figure S1). These results further suggest that Aki1 may be involved deeply in signal transduction through mutant EGFR.

Specific downregulation of *Aki1* inhibits cell viability and induces cell apoptosis in *EGFR* mutant lung cancer cells

To determine the role of Aki1 in *EGFR* mutant lung cancer cell lines, we used specific small interfering RNA (siRNA) for *Aki1* knockdown. Treatment with *Aki1*-specific siRNA suppressed Aki1 protein expression, and more decreased the viability of *EGFR* mutant cells (PC-9, HCC827 and H1975) than *EGFR* wild-type cells (A549 and PC14PE6) (Figure 2a and Supplementary Figure S2). To confirm the specificity of the *Aki1* siRNA used, we constructed RNA interference (RNAi)-resistant *Aki1* cDNA by mutating the sequence targeted by *Aki1* siRNA without changing the amino acid sequence. Transfection of wild-type *Aki1* or RNAi-resistant *Aki1* resulted in increased expression of Aki1 protein in PC-9 cells (Supplementary Figure S3A). Treatment with *Aki1* siRNA attenuated Aki1 protein expression and cell viability in parental and even in wild-type *Aki1*-transfected cells (Supplementary Figures S3B and C). However, *Aki1* siRNA did not downregulate exogenous Aki1 in RNAi-resistant *Aki1* cDNA-transfected cells. Transfection of RNAi-resistant *Aki1* cDNA overcame the *Aki1* siRNA-mediated decrease in cell viability (Supplementary Figure S3C), indicating the specificity of siRNA to *Aki1*. On the other hand, the effects of *Aki* siRNA in lung fibroblasts, MRC-5 and IMR-90, were only marginal (Figure 2a), suggesting that Aki knockdown selectively inhibits viability of cancer cells with dependent EGFR signal, especially in *EGFR* mutant lung cancer cells. In addition, to rule out any bystander effect of the siRNA, we performed cell culture using two color labeling. We found that *Aki1*-1 siRNA did not show any discernible bystander effect. Therefore, we conclude that the bystander effect is not the primary mechanism by which the *Aki1*-1siRNA treatment inhibited tumor cell growth, under our experimental conditions (Supplementary Figure S5A and B). Therefore, we focused solely on EGFR mutant lung cancer cells. Western blotting analyses indicated that *Aki1* knockdown reduced phosphorylation of downstream molecules, Akt and S6, and increased the levels of the proapoptotic molecule, cleaved PARP (poly (ADP-ribose) polymerase; Figure 2b), consistent with the decrease in cell viability. Furthermore, we also found that knockdown of *Aki1* discernibly induced apoptosis in PC-9, HCC827 and H1975 cells (Figure 2c).

We next assessed the effect of Aki1 inhibition, in comparison with EGFR inhibition, in *EGFR* mutant lung cancer cell lines. Like *EGFR* knockdown and erlotinib, *Aki1* knockdown considerably inhibited viability of PC-9 and HCC827 cells with exon 19 deletion in *EGFR*. In addition, *Aki1* knockdown inhibited viability of H1975 cells with exon 21 L858R and exon 20 T790M double mutations as potently as *EGFR* siRNA, whereas erlotinib had no effect (Figures 3a and b). These results suggest that targeting of Aki1 may be valuable for treating *EGFR* mutant lung cancer cells, especially with T790M gatekeeper mutation.

Aki1 knockdown inhibits tumor growth of lung cancer with EGFR T790M secondary mutation *in vivo*

Next, we examined the antitumor potential of *Aki1* siRNA against H1975 cells with *EGFR* T790M gatekeeper mutation *in vivo*. Intratumoral injection of either scramble or *Aki1* siRNA complexed with invivofectamine was performed on days 5 and 8. In a previous report, *MAGE-D1* gene knockdown by three direct injections of siRNA complicated with invivofectamine into the local region indicated 50% inhibition of protein expression.[26] *Aki1* siRNA treatment dramatically inhibited tumor growth in comparison with control or scramble siRNA (Figures 4a and b). We confirmed knockdown of Aki1 and the inhibition of downstream signaling molecule, S6, in tumors by western blotting (Figure 4c). These results clearly indicated the therapeutic potential of *Aki1* siRNA against lung cancer with *EGFR* T790M mutation *in vivo*.

Combined Aki1 and *EGFR* blockade strongly suppressed cell viability of lung cancer cells with *EGFR* T790M secondary mutation

Irreversible EGFR-TKIs and mutant selective EGFR-TKIs were developed to overcome *EGFR* T790M gatekeeper mutation-mediated resistance to erlotinib and gefitinib. Here, we examined whether Aki1 knockdown could augment the therapeutic efficacy of these new generation EGFR-TKIs. Irreversible EGFR-TKI, CL-387,785 and BIBW2992, and the mutant-selective EGFR-TKI, WZ4002, reduced the viability of H1975 cells, whereas erlotinib had no such effect. *Aki1* knockdown suppressed cell viability and further augmented the various dose inhibitory effects of CL-387,785, BIBW2992 and WZ4002 (Figure 5a and Supplementary Figure S4). Consistent with these findings, *Aki1*